Tampere University

Moeinreza Golzadeh

EIGEN ZERO-FORCING BEAMFORMING IN MU-MIMO 5G DOWNLINK

Fixed-Point Modeling

Information Technology and Communication Sciences (ITC)
Master of Science Thesis
March 2021

ABSTRACT

Moeinreza Golzadeh: Eigen Zero-Forcing Beamforming in MU-MIMO 5G downlink
Master of Science Thesis
Tampere University
Wireless Communications and RF Systems
March 2021

Multi-User Multiple-Input Multiple-Output (MU-MIMO) scheme serves several users simultaneously using same time-frequency resources and it achieves a larger capacity comparing to Single-User MIMO. Spatial multiplexing requires beamforming techniques and the weights are adjusted by linear precoding to mitigate inter-user interference. A possible method in 5G New Radio is Eigen-based Zero-Forcing (EZF) beamforming which is optimum in terms of computational complexity.

This thesis work aims to model a hardware accelerator for EZF downlink beamforming at the base station transmitter. Additionally, a computationally-optimized version of EZF beamforming is also modelled. Hardware implementation requires fixed-point modelling of both beamforming methods and the models are developed using 16-bit data accuracy.

System performance is compared between floating-point and fixed-point models for both EZF beamforming methods. The new data format results in a negligible performance loss, which indicates a fair tradeoff between implementation complexity and system performance.

Thesis framework is defined and developed at System-on-Chip (SoC) department of Nokia Networks in Tampere, Finland.

Keywords: Eigen Zero-Forcing Beamforming, 5G Downlink Precoding, MU-MIMO, Hardware Accelerator, Fixed-Point Modeling

PREFACE

I would like to express my appreciation to my supervisors Erno Salminen at Nokia Networks who was instrumental in progress of this thesis work, and Jukka Talvitie at Tampere University whose supports and feedbacks can't be overestimated.

Special thanks to my line manager Petri Kukkala and also Olga Kayo, who dedicated a time slot for doing my thesis besides my working tasks. I gratefully acknowledge the assistance of my colleagues Muhammad Waheed, Mohammad Majidzadeh, Stefan Wesemann, Alaaeddin Loulou, and others with their helpful contributions. Thanks should also go to Valtteri Tervo who defined the topic of this thesis.

I wish to thank my lovely friends for their supports during the pandemic time, kept me motivated towards the finishing line and made the path more joyful with their presence.

Finally, I'd like to extend my deepest gratitude to my wonderful family for their pure love and vital role in my life and my academic career. It would be burdensome to fulfill my master's degree without their overwhelming encouragements.

Tampere, 20th March 2021

Moeinreza Golzadeh

CONTENTS

LIST OF FIGURES

LIST OF TABLES

LIST OF SYMBOLS AND ABBREVIATIONS

3GPP	third generation partnership project
5G	5th generation of mobile communications
A/D	analog to digital
ASIC	application-specific integrated circuit
BER	bit error ratio
BF	beamforming
BS	base station
BTS	base transceiver station
$\mathbf{C}$	channel capacity
$\mathbb{C}$	complex numbers
CPU	central processing unit
CSI	channel state information
CSI-RS	CSI reference symbol
D/A	digital to analog
DL	downlink
DPC	dirty paper coding
DSP	digital signal processor
EBB	eigen-based beamforming
EVD	eigen value decomposition
EZF	eigen-based zero-forcing
FDD	frequency division duplex
FFT	fast Fourier transform
FLP	floating-point
FPGA	field programmable gate array
FR1	frequency range 1
FR2	frequency range 2
FXP	fixed-point
gNB	next generation NodeB (5G base station)
$\mathbf{H}$	channel matrix

$\mathbf{H_k}$	sub-channel matrix of user k
HLS	high-level synthesis
$\mathbf{I_r}$	identity matrix of size r
I	in-phase
IFFT	inverse FFT
IP	intellectual property
K	number of users
λ	eigenvalue
Λ	eigenvalues matrix
LC EZF	less computation-intensive EZF
LTE	long-term evolution
M	number of BS transceiver antennas
MCS	modulation and coding scheme
MIMO	multiple-input multiple-output
MU-MIMO	multi-user MIMO
N_{col}	number of BS vertical antenna elements
N_{pol}	number of BS antenna polarizations
N_{row}	number of BS horizontal antenna elements
$\mathbf{n}_k$	received noise samples at user k
NR	New Radio
OFDM	orthogonal frequency-division multiplexing
Q	quadrature-phase
QAM	quadrature amplitude modulation
QoS	quality of service
L	number of user data layers
$\mathbb{R}$	real numbers
RF	radio frequency
R	number of BS receiving antennas
ρ	receiver SNR
$\mathbf{R}_k$	channel covariance matrix
RX	receiver
SCS	sub-carrier spacing
SINR	signal to noise plus interference ratio
$\mathbf{s}_k$	transmitted data for user k

SNR	signal to noise ratio
SRS	sounding reference signal
SVD	singular value decomposition
T	number of BS transmitting antennas
TAU	Tampere University
TDD	time division duplex
TRX	transceiver
TUNI	Tampere Universities
TX	transmitter
$\mathbf{U}$	left-singular vectors
UE	user equipment
UL	uplink
ULA	uniform linear array
$\mathbf{V}$	right-singular vectors
$\mathbf{W}$	beamforming weights matrix
ZF	zero-forcing

1 INTRODUCTION

Wireless communications systems evolve towards higher data rates and challenges related to transmission power, bandwidth, and system complexity arise in return. This ever-growing demand for performance enhancement is accompanied by larger number of communicating device, resulting in more crowded communication channels. Beamforming is a promising solution in modern communication systems to utilize the communication channel more efficiently, by allowing multiple transmissions simultaneously and boosting the system performance.

This thesis presents the performance difference of two modeling approaches for downlink (DL) beamforming, using fixed-point (FXP) and floating-point (FLP) data types. Studied wireless system is the 5-th generation of mobile communications (5G) cellular system. The goal of the transmitter side DL beamforming is to concentrate transmitting power from the base station (BS) to the target user equipment (UE) direction and at the same time, to reduce interference with other users. This directivity at the receiver side can be used to enable spatial multiplexing, establishing multi-layer transmission in parallel by using shared resources [4].

A multiuser multiple-input-multiple-output (MU-MIMO) system model is carried out in this thesis and eigen-based zero-forcing (EZF) the studied beamforming method. Moreover, impact of data types is analyzed and a new less computation-intensive EZF beamforming method (LC EZF) is developed and compared to the earlier method.

Previous research works attempt to either model zero-forcing beamforming methods including EZF in only FLP data precision, or they concentrate largely on FXP implementations. The novelty with this thesis work is to study the performance loss from data impact of FXP model on FLP reference model. The outcome can be beneficial to hardware resource planning in telecommunications industry, where the hardware realization of the system is expected to satisfy the performance criteria. The continuation of this section delivers a general understanding of 5G technology and data formats used in signal processing. Later on, section 2 concentrates on beamforming algorithms and multiuser communications channels characteristics. Section 3 is dedicated to the system model and mathematical points of view regarding eigen-based and ZF beamforming. Simulation scenarios are presented in section 4, and the results are presented in section 5 where performance of FLP model and FXP model are compared.

Figure 1.2 summarizes all of the major steps done in this thesis work, starting from getting

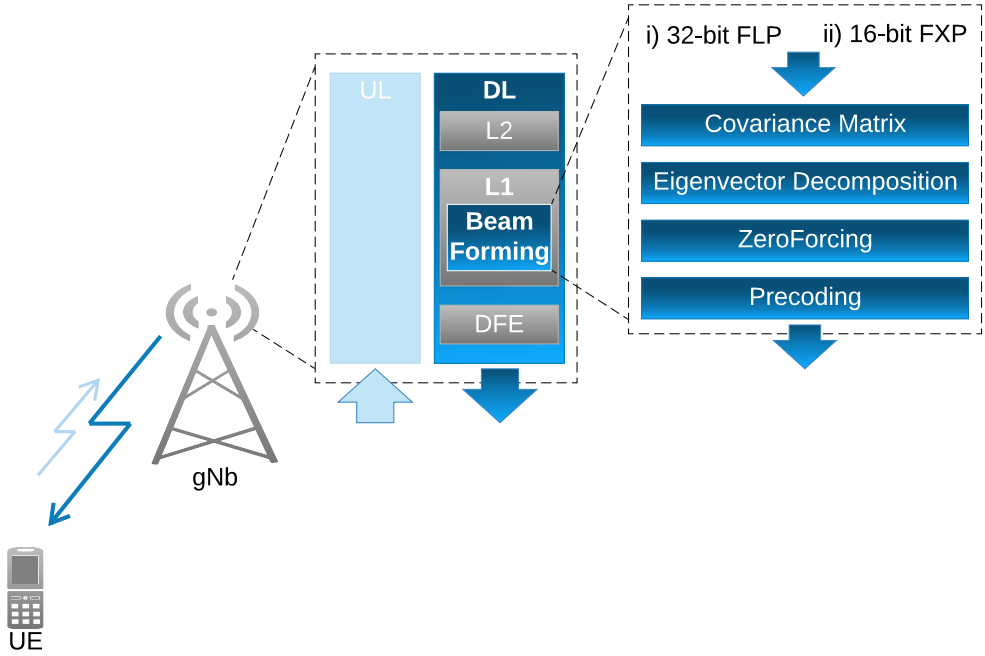

Figure 1.1. *An overview of the studied downlink beamforming model.*

known to the Nokia Networks internal simulation environment, creating simulation scripts to test the effects of various parameters, implementing a new FLP model for LC EZF beamforming, creating fixed point model out of EZF and LC EZF FLP models, and eventually to investigate data format impacts on different simulation parameters. Statistical results linked to possible performance loss is represented at the end of this document.

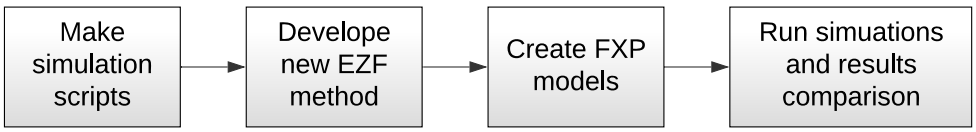

Figure 1.2. *Summary of steps taken in this thesis work.*

1.1 5G New Radio

5G New Radio (NR) services are mainly categorized into three classes shown in fig. 1.3: enhanced Mobile Broadband (eMBB), Ultra Reliable and Low Latency Communications (URLLC), and massive Machine Type Communications (mMTC).

A few use cases are listed below, however some examples may belong to other targets as well:

- eMBB: Virtual Reality (VR), Virtual meetings, UHD video streaming, video monitor-

ing.

- URLLC: public safety, remote surgery, vehicle to vehicle (V2V) communications, industrial automation.
- mMTC: wearables, healthcare monitoring, smart home and smart cities.

Propagating channels that 5G services operate in are one of major limiting factors in 5G system performance [30]. Thus, it's of importance to investigate about channel characteristics including massive MIMO, multi-user MIMO (MU-MIMO), millimeter-wave (mm-Wave) bands, and 3GPP spatial channel models. 5G networks offer larger network capacity and massive MIMO as a key enabler expands system capacity while it saves the cost of deploying more BS units. 5G mm-Wave frequency spectrum delivers extreme capacity, ultra-high throughput, and ultra-low latency. Mm-Wave transmission operates above 24GHz and it utilizes massive MIMO antennas to enable larger antenna arrays within smaller space.

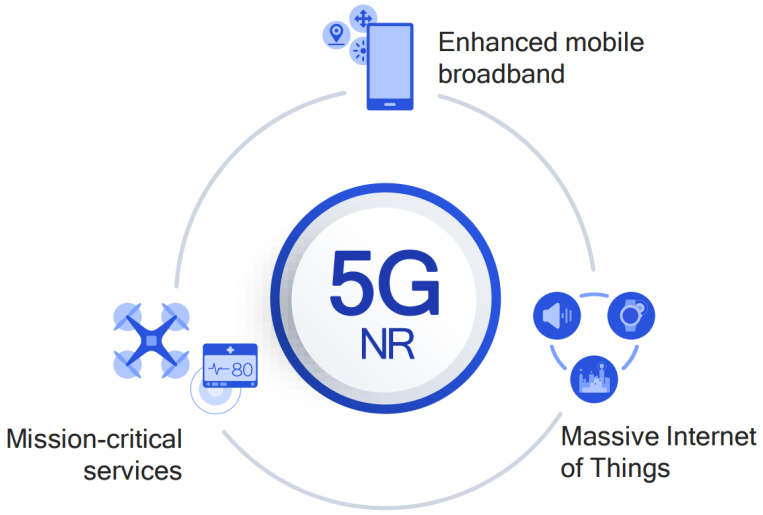

Figure 1.3. *5G NR backbones: eMBB, URLLC, and mMTC [image: Qualcomm].*

DL transmission is about the streaming signal coming from the base transmission system (BTS or BS) and propagated towards the user equipments (UE). From baseband signal processings at 5G BTS (gNB) to tackle channel impacts in downlink direction, linear precoding is an efficient practical choice due to a good balance between system performance and complexity. Zero-forcing beamforming is a well-known beamforming among linear precoders and can be used with digital beamforming methods. With eigen-based beamforming, higher orders of channel statistics can be considered, when exploiting channel characteristics for beamforming purposes.

1.2 Fixed-point and floating-point

Digital signal processing (DSP) can be done in two basic flavours: fixed-point and floating-point numbers. The main advantage of using floating-point is higher accuracy, which

allows to discard scaling concerns. However, floating-point processing needs larger silicon area which is the area of semiconductor components in practical implementation of a DSP block, and it also runs slower on a fixed-point CPU, by a factor of two as an example.

Designers have to pay attention to the limitations of the fixed-point number systems, including prevention of overflow and precision conservation by scaling the signals [17]. Analog-to-digital (A/D) and digital-to-analog (D/A) conversion and multiplication are two sources in which quantization errors cause precision loss. Figure 1.4 shows an example of a sine wave before and after passing through a quantizer block. Since multiplication exists in all DSPs, discarding any of the bits from full precision numbers creates information loss.

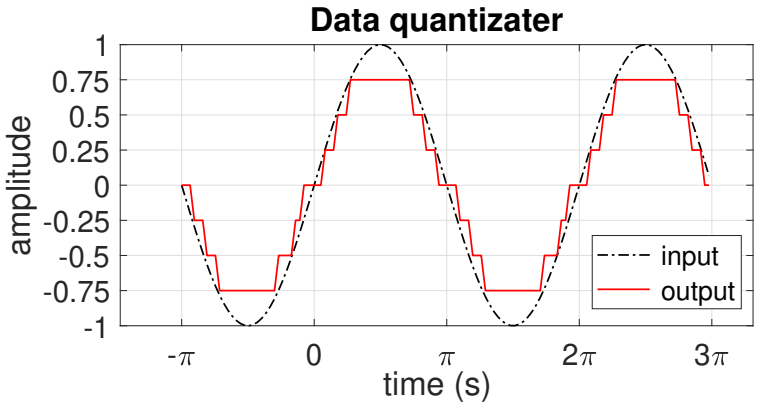

Figure 1.4. *Impact on input signal to a quantizer block, with 0.25 quantizating steps.*

A large number of DSP system models require non-linear datapaths implementation on field-programmable gate array (FPGA) and application-specific integration circuit (ASIC) hardwares with a high resolution floating-point format e.g. 64 bits in reference models [28]. Assumption of having readily high or infinite precision is possible, but this is not affordable in terms of ASIC/FPGA direct implementations.

Nevertheless, lower cost, less power consumption, and faster processing speeds make fixed-point DSPs frequently preferred over floating-point processors [24]. Floating-point functions require more logic gates. These factors, plus greater number of pins required by the wider data bus, results in a larger die and a bigger package that leads to a significant cost premium for the new floating-point devices [8]. One practical way of reducing such programming complexities of FXP is utilizing high level languages, however due to large overhead in executing FLP operations using FXP data path, it's not the best choice.

Hardware implementations of wireless communication algorithms is no exception here and it's in need of FXP arithmetic, however, most of these algorithms are developed in FLP arithmetic [44]. A key step for High-level synthesis (HLS) is automation of FLP to FXP transformation, or bit-width optimization.

2 BEAMFORMING

Wireless communications systems evolve towards higher and higher data rates and challenges related to limitations of power, bandwidth, and complexity arise [10]. Multiple-access interference limits the capacity of mobile communication systems, and to attain a given service quality, increasing the required transmission power is harmful [41]. Moreover, 5th generation of mobile communications network (5G) New Radio (NR) uses higher frequency ranges than earlier standards, as shown in Fig. 2.1. Propagation loss in mmWave transmission in frequency range 2 (FR2, above 6 GHz) plays a significant role and must be compensated. This can be done by utilizing massive MIMO systems or beamforming techniques to increase the spectral efficiency.

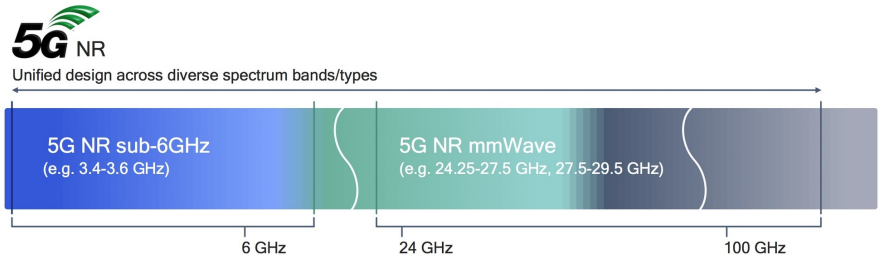

Figure 2.1. *5G NR frequency bands [image: Qualcomm].*

However, the cost of this increased performance is the additional cost of deploying multiple antennas, the space requirements of these extra antennas especially on small handheld UE, and also the extra complexity which is required for multi-dimensional signal processing. At higher frequencies (lower wavelengths) an antenna array takes smaller physical space which reduces element spacing and element size of antennas.

This thesis concentrates on digital downlink transmitter side beamforming which is a baseband (BB) processing unit before the radio frequency (RF) transmission modules.

2.1 Multiple input, multiple output (MIMO) channels

Multiple-input, multiple output (MIMO) simply means that many antennas are used in wireless communication at both transmitter and receiver sides, as illustrated in Fig. 2.2. Delay constraints limits the usage of time diversity and therefore antenna diversity, or similarly spatial diversity, is obtained through placing multiple antennas at the transmitter and/or the receiver [38].

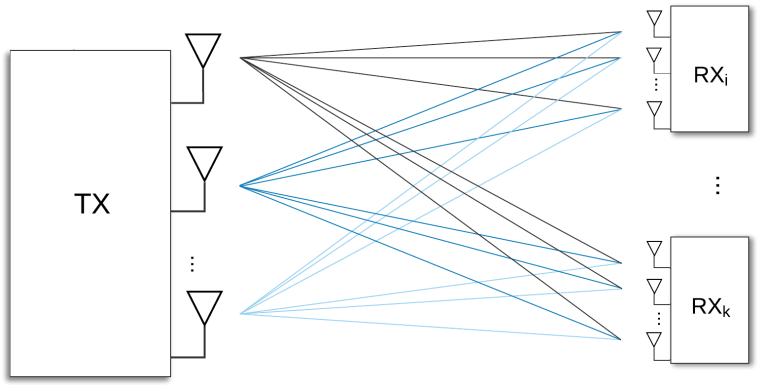

Figure 2.2. *MIMO channel and system block diagram*

BS with many antennas, due to the asymptotic orthogonality between MIMO channels, allows to remove significantly inter-user interference as well as delivering larger capacity gain [5]. Higher spatial efficiency is achieved too by higher number of antennas.

With a sufficient antenna separation, for example half of the wave length, channel gains between different antenna pairs experience almost independent fading. Receiver combines data from many RX antennas to create a better quality signal than any of them alone.

Fig. 2.3 illustrates so called "local scattering environment" where the transmitted signal is affected by numerous obstacles independently. Signal propagates through many routes and each experiences different conditions and delays. Therefore, the mobile radio channel can be modeled as a wide-sense stationary uncorrelated scattering channel [43]. Rich scattering environment provides independent and uncorrelated paths from each transmitting antenna to each receiving antenna [10]. MIMO channel capacity is heavily dependent on antenna element correlations of the channel and accordingly, antenna correlation changes drastically with variations in scattering. Channels with rich scattering provide a remarkable spectral efficiencies for MIMO.

MIMO can increase the data rates without increasing the transmitting power or bandwidth [12]. MIMO systems can be configured for different modes of spatial diversity, beamforming, multiplexing, and spatial multiple access, based on the channel condition [21]. Maximum achievable diversity gain of a MIMO system is equal to the number of independent antenna paths, and minimum of transmitter/receiver antenna numbers is same as maximum number for supported spatial streams [19].

Moreover, maximum theoretical throughput of a MIMO system increases linearly with multiple number of simultaneous UEs. This can be achieved by a scheme called dirty paper coding (DPC) which is based on interference pre-subtraction, whilst a trade-off between system complexity and performance should be considered. When the number

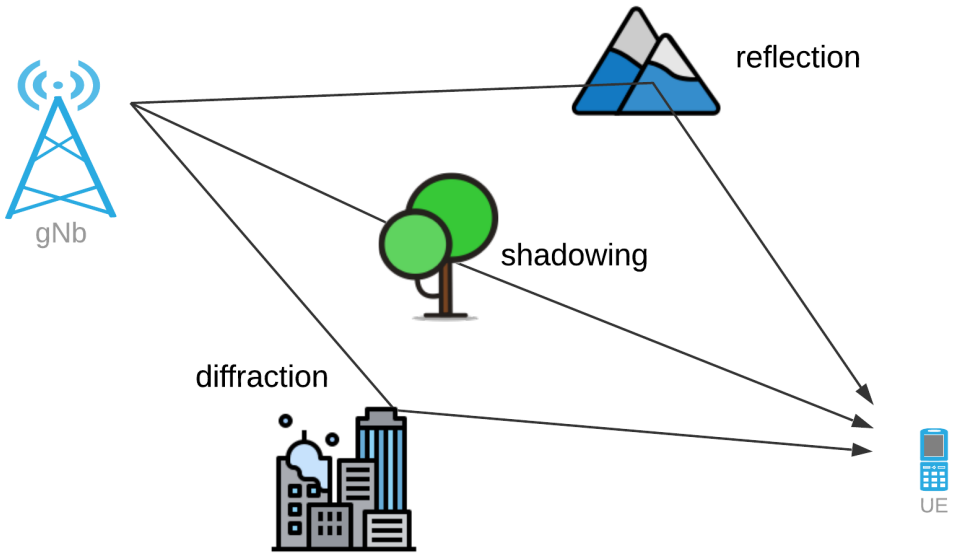

Figure 2.3. *Multipath components: shadowing, slow and fast fading.*

of UEs exceeds the number of transmitting antennas, there would be a linear increase in the capacity regardless of number of UE's receiving antennas [36]. However, even if DPC is an optimal method for MIMO downlink, it has such a large computational complexity that it is difficult in practice.

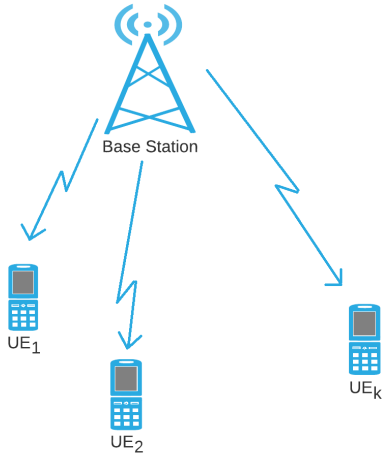

Figure 2.4. *Multi-user MIMO channel downlink transmission.*

In multi-user MIMO (MU-MIMO) systems, different users are allocated to same frequency band and have overlapping resource blocks. Multi-user means several UEs are served simultaneously over a given time-frequency resource using spatial multiplexing, as shown in Fig. 2.4 [29]. System performance of a conventional MU-MIMO communication link is noticeably affected by inter-user interference. Sources of an incoming desired signal and

an interfering signal are located in different spatial locations usually, and this can thus be taken in to account to separate the signals and filter out unwanted signals.

Research has focused on two optimization problems related to MU-MIMO channels [35], namely:

1. power control - minimize the total transmitting power providing a minimum Quality-of-Service (QoS) level
2. throughput maximization- maximize the sum of information rates of all UEs for a given power limit

2.2 Channel state information (CSI)

Both the BS and the UE send known reference symbols periodically so that the receiver can estimate the channel conditions. Channel state information (CSI) is derived from the estimated channel conditions and it's transmitted in both directions via a control channel. It describes known channel properties of the radio link while characterizing the path loss, scattering, diffraction, fading, shadowing, etc [20]. Accurate CSI enhances MIMO system performance and capacity [33].

Since the wireless channel is time-variant and frequency-selective, reaching close to Shannon maximum channel capacity is difficult if CSI is absent at the transmitter [15]. Additionally, CSI must be sent back to the transmitter first, prior to where precoding data takes place, and then CSI can be used to encode the UEs data and it is called a close-loop CSI acquisition, as discussed in more detail in section 2.2.1. If the transmitter has knowledge of the CSI, higher channel capacity can be achieved by utilizing adaptive coding method and allocating the power to the right singular subspace of the channel matrix derived in section 3 [11].

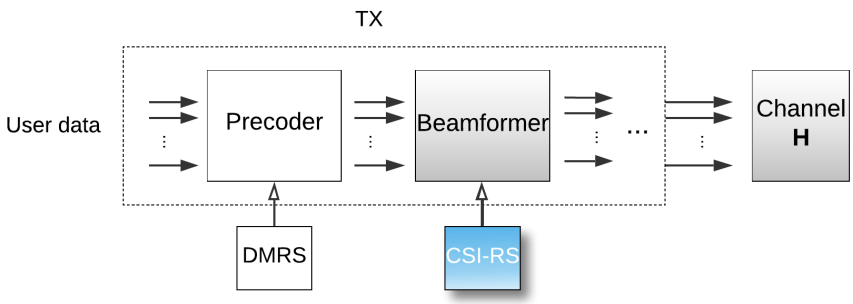

Figure 2.5. *Some reference signals and their impacting place on the transmitter processing blocks.*

CSI may consist of several components in 5G New Radio that has been discussed in 3GPP 138.214 (V 15.3.0) and they are listed briefly as follows:

- channel quality information (CQI)

- precoding matrix indicator (PMI)
- CSI reference signal (CSI-RS) resource indicator (CRI)
- SS/PBCH block resource indicator (SSBRI)
- layer indicator (LI)
- rank indicator (RI)

Fig. 2.5 shows two types of downlink reference symbols used by the UE to estimate the channel condition. Both demodulation reference signal (DMRS) and CSI-RS help UE to figure out about the TX matrices of precoder and beamforming, as well as channel. 5G supports the following reference signals for NR uplink in multi-antenna schemes [1]:

- SRS: Sounding Reference Signal, with main functionalities of beam management and CSI acquisition.
- DMRS: reference signal that takes care of data and control demodulation.
- PTRS: Phase tracking reference signal.

Receiver can estimate the channel correlations by taking long-term averaging of the channel instances, and report them as a feedback to the transmitter using a reliable low-rate channel [33]. In TDD systems, transmitter can also get the channel statistic info directly, because almost same physical channel characteristics exist in both UL and DL, even though by considering transmission time delay between UL and DL. In FDD cases considering small spreading angle, DL channel covariance estimate is precisely calculated from UL channel covariance using frequency calibration processing.

Transmission power or direction is changed according to the CSI in a transmission, and *eigen-beamforming* (EBB) is a typical technique used in such transmissions [18]. Channel covariance matrix provides longterm and wideband feedback and each UE provides a quantized version of the covariance matrix. This quantization is based on a set of orthogonal basis vectors whose quantity equals to the number of supported simultaneous beam pair links.

2.2.1 Open-loop and Closed-loop CSI acquisition

There are two common ways of obtaining CSI reports as shown in Fig. 2.6: open-loop and closed-loop [26]. Open-loop transmission relies heavily on the channel condition in uplink and downlink to be highly correlated and channel reciprocity plays a key role there. Receiver alone does the channel estimation which results in more complexity and less channel diversity. Closed-loop CSI acquisition depends on the receiver estimation capabilities and receiver estimates the channel response and feedback is sent back to the transmitter through a limited feedback channel.

A closed-loop approach utilizes receiver feedback to estimate CSI and then by processing the CSI at the transmitter (CSIT), beamforming can be performed to distinguish MU-MIMO channel UEs [7]. On the other hand, an open-loop scheme uses predefined

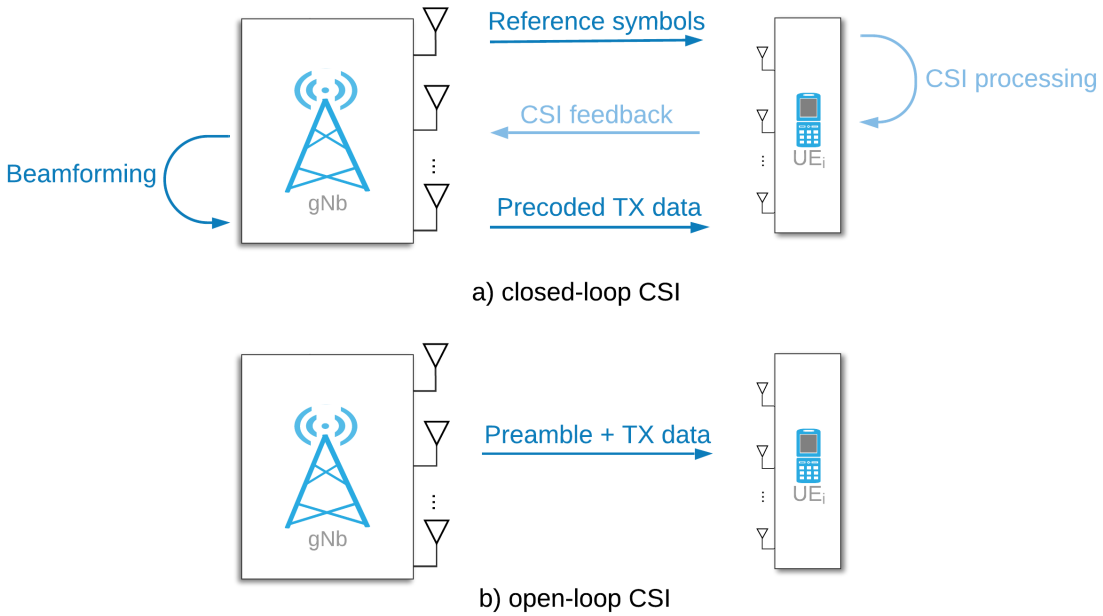

Figure 2.6. *Closed-loop and open-loop CSI acquisition between transmitter and receiver [7].*

preamble sequences, tansmitted along with the UE data, to estimate the unknown channel through those known preamble set. In open-loop systems, transmitter may not fully consider the inter-user interferences and transmitted streams can be propagated through correlated channels.

Some obstacles make it hard to calculate CSIT in closed-loop systems, namely limited feedback resources, delay of feedback signalling, and scheduling delay with small channel coherence time [40]. Open-loop systems also suffer from antenna calibration errors and turn-around time delays. Utilizing of CSI reports allocates some of channel bandwidth that reduces the overall capacity [15]. CSI doesn't always reflect the current channel state due to the feedback channel delays and only imperfect CSI report is available at the transmitter.

Providing CSI feedback by transmitter in rapidly varying channels (relative to the speed of feedback channel) is costly and not always meaningful to acquire instantaneous CSI, since optimal transmissions that are tuned to an older CSI information become out-of-date pretty fast [33]. Accordingly, feedbacks based on statistical information of the underlying stationary random channels are proposed. Transmitter can obtain this statistical a priori through some field measurements, ray-tracing simulations, or physical channel modellings [31].

Since CSI in rapidly varying channels may be costly or impossible to acquire and water-filling based approaches can be used which requires only channel correlation updates, without exceedingly fast updating rate [33]. Systems operating in frequency division duplexing use different frequency bands for uplink and downlink which results in non-reciprocal channel response and are therefore limited to use closed-loop CSI.

2.3 Beamforming concept

Beamforming (BF) is a sub-optimum solution to serve multiple UEs at the same time, but with a reduced computational complexity compared to DPC. The term beamforming comes from spatial filtering that is used to receive a transmitted signal of interest and cancel out unwanted signals, so-called interfering signals [39]. In this context, multiple antennas at the transmitter are used to obtain diversity gain rather than capacity gain [12]. Providing diversity against fading is also realized by multiple transmitting/receiving antennas, through either of inter-antenna spacing or different polarizations [4].

Beamforming uses independent coding for each UE stream. User data is multiplied by beamforming vectors, so that they combine coherently in certain direction when it is sent through multiple transmitting antennas. Spatial separation between UEs is taken into account for beamforming weight vectors so that inter-user interference can be reduced or removed. It is also stated that with optimal BF vectors, as the number of UEs increases toward infinity, BF performance approaches to that of DPC method [32].

2.3.1 Beamformer types

Beamforming can be utilized in both receiver and transmitter sides, and complex base-band weights of the transmitting and/or receiving data adjust and shape the beams so that signal-to-interference-and-noise ratio (SINR) in increased at each antenna element [21]. Same symbols is sent over each transmitting antenna using a weighted scale factor, and at the receiver side, all received signals are coherently combined using a different scaling factor to maximize the received SNR, so called *beamforming gain* [2].

Beamformers can be classified in two methods of data independent and statically optimum. In the latter, beamforming weights are chosen based on statistics of the data array, namely second order statistics of the received data. They can be also classified into three methods, as shown in Fig. 2.7:

1. Digital
2. Analog
3. Hybrid.

Pure digital beamforming is done using digital signal processors which gives huge flexibility towards implementing efficient beamforming algorithms with higher degree of freedom. However, each antenna elements requires a separate RF chain and this brings complexity in the receiver architecture and high power consumption. In the analog beamforming, time delay elements or phase shifting of the signal are considered before/after RF up-conversion steps, in order to adjust the antenna weights. Hybrid beamforming combines both analog and digital beamformig techniques to improve performance of analog and reduce complexity of digital method, and hybrid beamformers can be divided into fully connected and partially connected types [27].

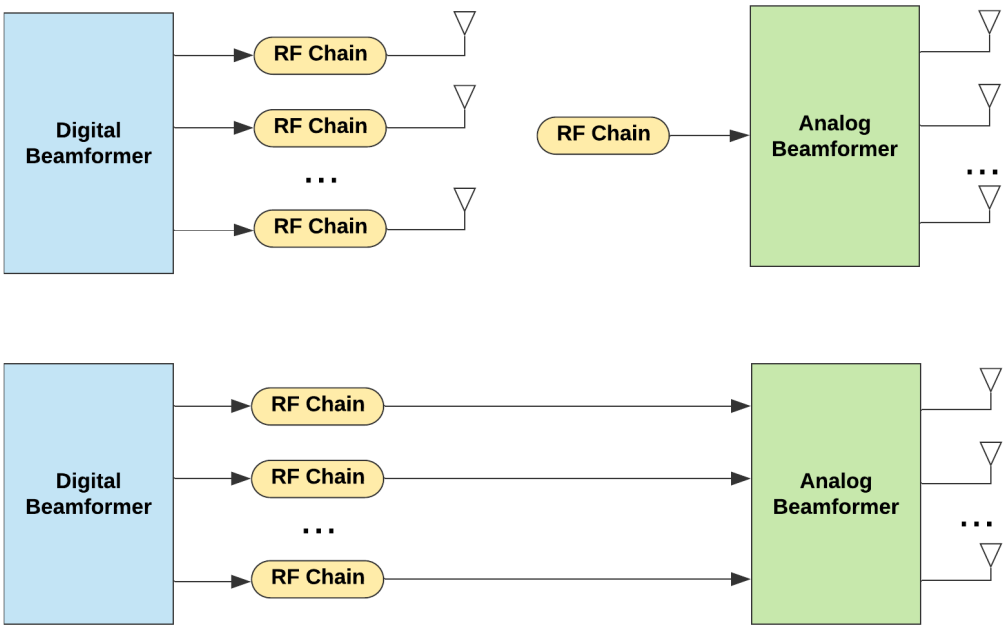

Figure 2.7. *Analog beamforming (top right), Digital beamforming (top left), and Hybrid beamforming (bottom) concepts.*

2.4 Basic beamforming algorithm

Fig. 2.8 shows the main steps of downlink digital beamforming. First the BS should estimate the channel matrix through reference signals. Transmitter uses sounding reference signal (SRS) that is available in the signal transmitted from the UE to the BS. SRS, as an input for beamforming or channel estimation, is used to monitor the uplink channel quality which is beyond the scope of this thesis. Next step is to compute covariance matrices (CoMa), or similarly correlation matrix, which makes a square matrix of channel estimates, whose dimension is equal to the maximum number of antennas at the BS. Later on, channel correlation is decomposed into eigenvector as one column vector of complex data, for each UE. Zero-forcing (ZF) is an optional step to improve inter-user interference performance and is applied to all user weights to make them as orthogonal as possible. Phases of the different antenna signals are adjusted by multiplying the beamforming weights with UE data. Afterwards, this result data goes through IFFT block which converts OFDM data to time-domain. After that data goes to digital-front end (DFE) and finally to DAC and TX antennas.

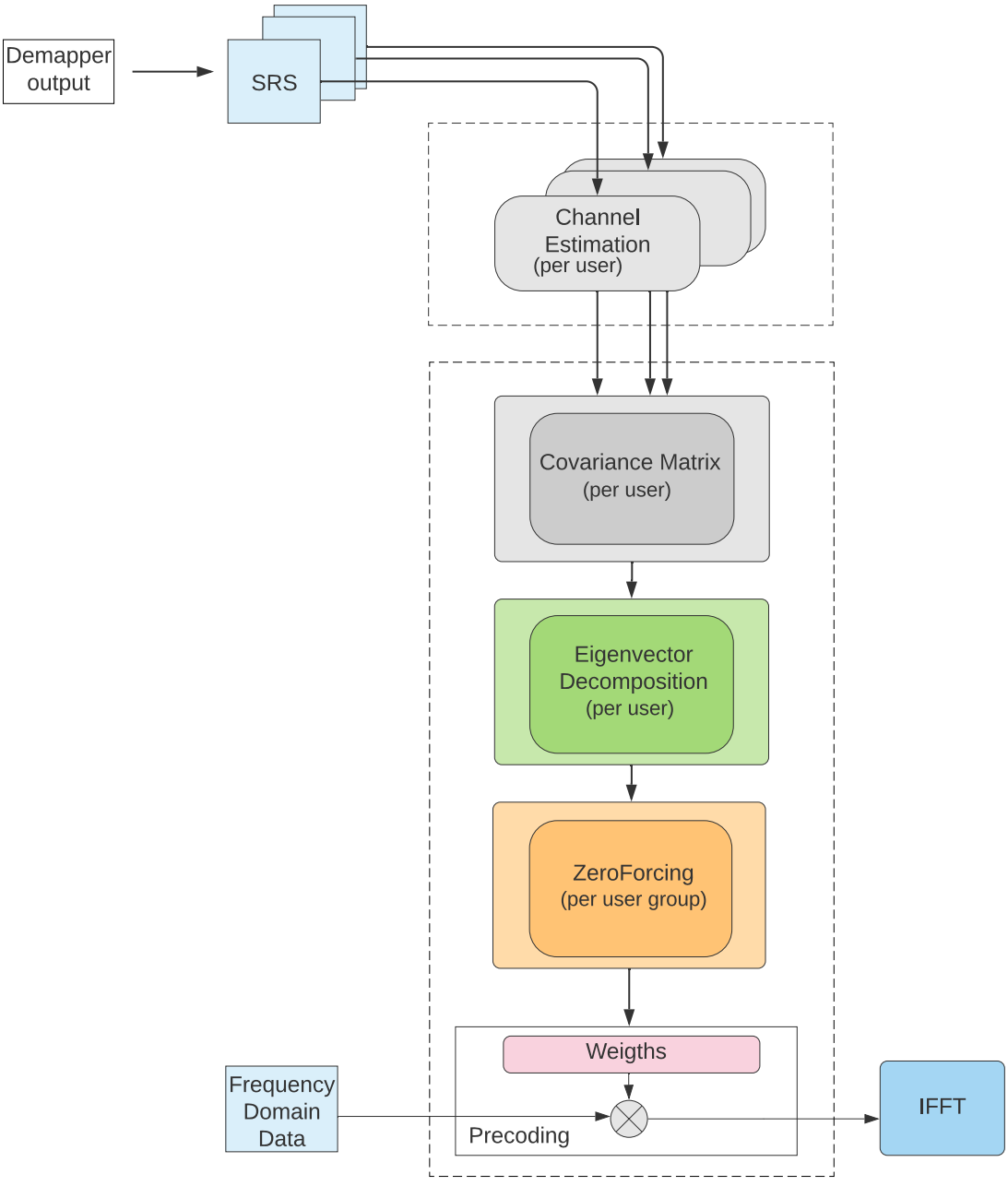

Figure 2.8. *Zeroforcing beamforming steps from channel estimation to precoding.*

3 SYSTEM MODEL

Assume that we have K UEs, M number of BS transceiver antennas, R receiving and T transmitting antennas ($T \leq R$) for each UE $(\text{here } T = R)$, and each UE has L data layer $(\text{for simplicity } L = 1)$.

Antenna elements at the BS are geometrically divided to N_{pol} polarization types, N_{col} vertical elements, and N_{row} horizontal elements. Accordingly, the uplink (UL) channel between each UE and BS would be $\mathbf{H}_k \in \mathbb{C}^{M \times T}$ and $M = N_{col} \times N_{row} \times N_{pol}$.

An example of BS antenna configuration is depicted in Fig. 3.1, with 4 rows ($N_{row} = 4$) and 8 column ($N_{col} = 8$) elements and 2 polarizations ($N_{pol} = 2$), in total $M = 64$ antenna elements.

Received signal $\mathbf{y}$ at UE k is defined as

$$\mathbf{y}_k = \mathbf{H}^H \mathbf{x}_k + \mathbf{n}_k \tag{3.1}$$

where ^{H} is Hermitian operator, $\mathbf{H} \in \mathbb{C}^{M \times R}$ is the full uplink channel matrix for all UEs, transmitted data matrix of $\mathbf{x}_k \in \mathbb{C}^{M \times 1}$ for UE k, and noise samples of $\mathbf{n}_k \in \mathbb{C}^{R \times 1}$.

Beamforming affects the transmitting signal $\mathbf{s_k}$ and we have

$$\mathbf{x}_k = \mathbf{W_k s_k} \tag{3.2}$$

where $\mathbf{W}_k \in \mathbb{C}^{M \times R}$ is the beamforming weights matrix and transmitted data matrix of $\mathbf{s}_k \in \mathbb{C}^{R \times L}$ for UE k with L=1.

Received signal $\mathbf{y}$ considering beamforming weights matrix can be re-written by substituting Eq. 3.2 into Eq. 3.1 as

$$\mathbf{y}_k = \mathbf{H}^H \mathbf{W}_k \mathbf{s}_k + \mathbf{n}_k. \tag{3.3}$$

Rest of this thesis work is dedicated to how to find these optimum beamforming weights of $\mathbf{W}_k$ for all UEs.

3.1 System capacity

Assuming that channel matrix $\mathbf{H}$ is known at both ends and the transmission experiences a flat channel response in the desired bandwidth, channel capacity can be written as

$$C = \log_2 \det \left[\mathbf{I}_r + \frac{\rho}{r} . \mathbf{H}^H \mathbf{H} \right] \text{bit/sec}, \tag{3.4}$$

where ρ is signal-to-noise ratio (SNR) at the receiver side and r is the minimum number of transmitting antennas or receiving antennas. By taking parallel decomposition of the channel matrix into account (described in the following sections), capacity would be simplified as

$$C = \sum_{i=1}^{r} \log \left(1 + \frac{\lambda_i P_i}{\sigma^2} \right), \tag{3.5}$$

where $r = \min(M, T)$ is rank of the channel described in section 3.2, λ_i is the i-th eigenvalue of Hermitian matrix of $\mathbf{H}^H \mathbf{H}$, σ^2 is channel noise power, and P_i is power allocation derived from *water-filling* method and $\rho = P_i / \sigma^2$ [3][37]. As shown in Eq. 3.5 for only a certain index i, channel capacity becomes similar to the one from flat fading or frequency-selective with constant channel gains [11].

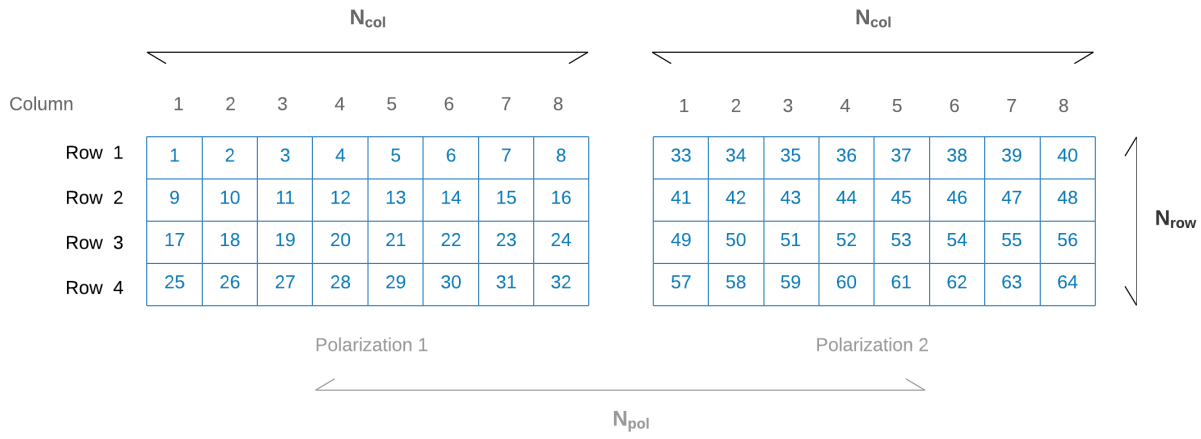

Figure 3.1. *Physical placement of BS antenna elements.*

3.2 Zero-forcing beamforming

Figure 3.2 illustrates the concept of eigen-based Zero-forcing (ZF) beamforming which is special form of our under-study linear precoding. Inter-user interference is forced to be the smallest towards each UE. In the same figure, sizes of the oval shapes represents the signal power in certain directions. The main lobe is the largest and each of them points roughly toward the desired UE. Each color represents different channel condition of different UEs they are experiencing, such that UE data is affected by their corresponding subchannel eigenvectors.

As an example, UE_1 undergoes subchannel $\mathbf{H}_1$ and its downlink data is enhanced along with subchannel $\mathbf{H}_1$, all represented in green color. Green main lobe is the largest comparing to other colors when passing through subchannel $\mathbf{H}_1$ and this is highlighted as the main point of zero-forcing which is to minimize side lobes in the directions that point to other UEs.

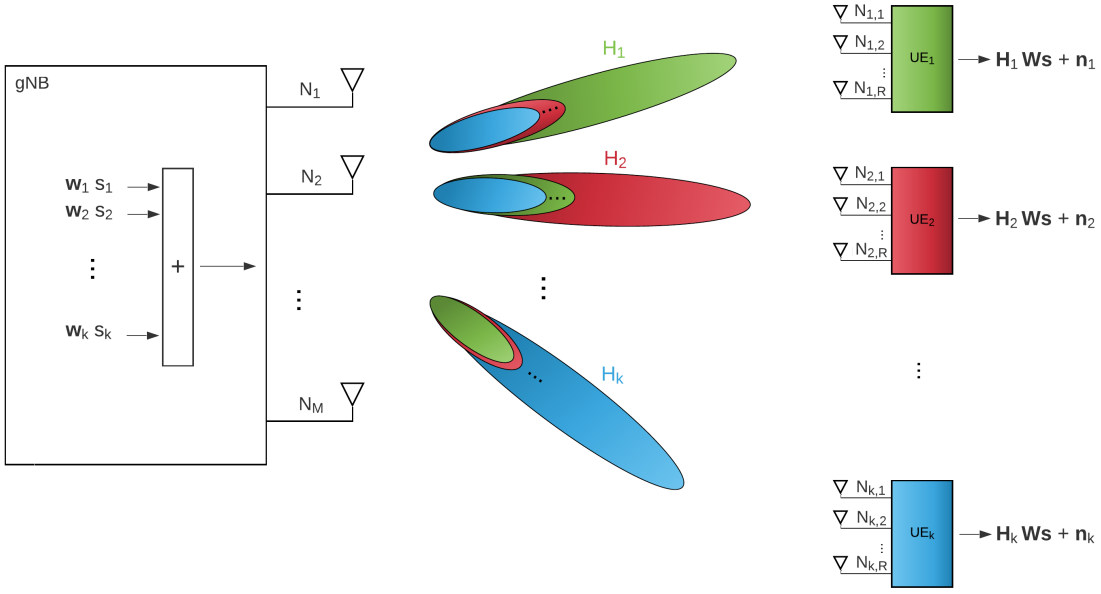

Figure 3.2. *Eigen-based beamforming concept in downlink MU-MIMO.*

Assume that rank of the channel matrix is defined as $\text{rank}(\mathbf{H}) = \min(M, T) = r$, data transmission can be performed over r parallel sub-channels [13]. If BS has channel state information report available, channel inversion (CI) can be performed at the BS. In channel inversion, or similarly ZF beamforming, user data vector is multiplied by the inverse of the effective channel matrix and therefore it acts as a channel equalizer [23]:

$$\mathbf{W} = \mathbf{H}_{eq}^{H} \left(\mathbf{H}_{eq} \mathbf{H}_{eq}^{H} \right)^{-1} \tag{3.6}$$

where $\mathbf{H}_{eq}$ is called the effective channel and is presented as $\mathbf{H}^{H}\mathbf{H}$ in Eq. 3.4.

ZF scale up the calculation performance by using frequency chunks of several subcarriers called physical resource block (PRB) that are more efficient in data transferring and on-the-fly calculations, when we compare it to do for every single subcarrier. Weight calculations for every single subcarrier takes a lot of time and the required performance goes out of hardware capabilities. By moving towards smaller coefficients calculation period, data buses and memory limits drags the granularity of data transferring rates.

There should be also a cap on size of the beamforming weights calculation in terms of subcarrier group size, e.g. maximum of 4 PRBs and it can be based on channel conditions and downlink signal setup.

This hardware limit is also a proof to why channel correlation is averaged over time or

even antenna groups based on polarizations, so that reduced channel dimension ease the burden of huge data computation loads.

Transmitting signals are pre-processed by effective channel pseudo-inverse so that data is reconstructed at the UE of interest and is forced to zero at all other antennas by destructive interference. Problems of CI as a linear method is increasing with transmitting power and sum rate restrictions [34].

Linear precoding schemes provides a promising tradeoff between complexity and performance of the transmitter design [42]. ZF beamforming is the most common scheme among linear precoding methods, however, it is a sub-optimal approach without any throughput maximisation. ZF decouples the MU-MIMO channel into several independent subchannels and the designing challenge would be reduced to power allocation problem.

Beamforming weights that are chosen carefully to omit inter-user interference between ongoing streams, take advantage of spatial separation between different UEs to support them simultaneously [36]. Space-division multiple access (SDMA) is the name of this multi-user communication scheme. Besides the complexity reduction in ZF, it can achieve a fairly large fraction of system capacity with DPC method in the situation that BS has multiple antennas and each UE has a single antenna. ZF also provides full degrees of freedom when SNR is high or there is a sufficiently large number of UEs.

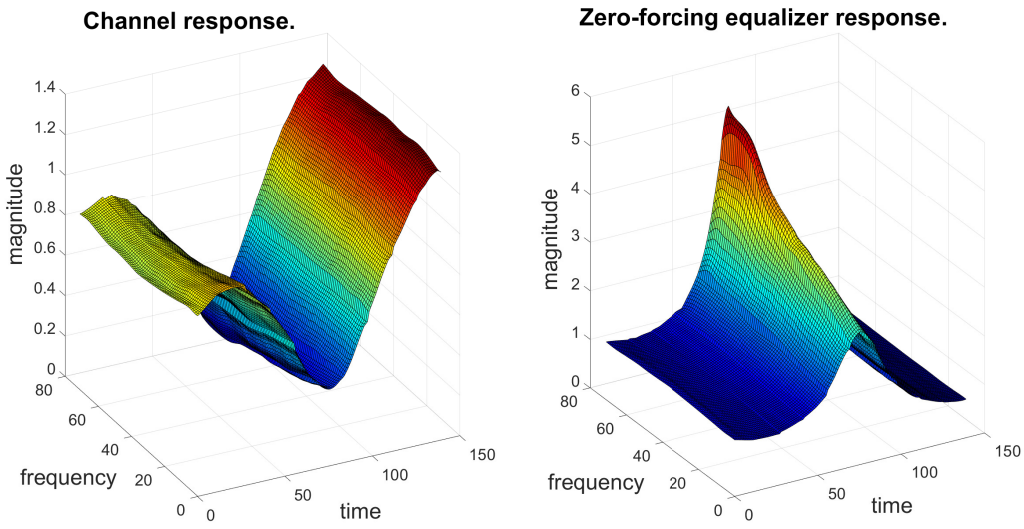

Figure 3.3. *Zero-forcing equalizer response for a random channel, in terms of time, frequency, and magnitude samples.*

After calculating effective channels for all UEs, we can take them and perform multi-user zero-forcing based on those extracted eigenvectors out of the channel covariance matrix.

Maximum Ratio Combining (MRC) is utilized at the UE side as the receiver diversity scheme. MRC is an optimum way of branch weighting that maximises the receiving SNR and it uses conjugate of the channel gains to combine incoming signals as in Eq. 3.7:

$$\mathbf{a}_i = \mathbf{g}_i^H = \alpha_i e^{-j\phi_i} \tag{3.7}$$

where $\mathbf{a}_i$ is the i-th combiner weight, and sub-channel gain is defined as $\mathbf{g}_i = \alpha_i e^{j\phi_i}$. If we suppose that received data vector for UE k is $\hat{\mathbf{s}}_k \in \mathbb{C}^{R\times 1}$ and MRC combining weights of $(\mathbf{H}_k\mathbf{w}_k)^H$, then we have

$$\hat{\mathbf{s}}_k = \mathbf{w}_k^H \mathbf{H}_k^H \left(\mathbf{H}_k \mathbf{W}\mathbf{s} + \mathbf{n}_k\right) \tag{3.8}$$

where $\mathbf{w}_k$ is beamforming vector of UE$_k$, $\mathbf{H}_k$ is channel matrix, and $\mathbf{n}_k$ is noise samples of UE$_k$, $\mathbf{W} = [\mathbf{w}_1, \mathbf{w}_2, \ldots, \mathbf{w}_K]$ is the beamforming weights matrix, and $\mathbf{s} = [\mathbf{s}_1, \mathbf{s}_2, \ldots, \mathbf{s}_K]^T$ is transmitted data for all UEs.

Now if we separate the transmit data for UE k from rest of the UEs, the first term in the following equation accounts for our UE of interest which should be the dominant term, and the second term, or similarly the inteference, should be nullified:

$$\hat{\mathbf{s}}_k = \mathbf{w}_k^H \mathbf{H}_k^H \mathbf{H}_k \mathbf{w}_k\, \mathbf{s}_k + \mathbf{w}_k^H \mathbf{H}_k^H \mathbf{H}_k \left(\sum_{i=1,\, i\neq k}^{K} \mathbf{w}_i\, \mathbf{s}_i\right) + \mathbf{w}_k^H \mathbf{H}_k^H \mathbf{n}_k \tag{3.9}$$

In the eigen-based beamforming, covariance of the channel frequency response is used to optimize beamforming response. Covariance of two random variables is a measurement of their joint variability, or similarly, their degree of association [25].

Channel covariance matrix, mentioned earlier in equation 3.4, is defined as

$$\mathbf{R}_{k,inst.} = \mathbf{H}_k^H \mathbf{H}_k, \;\; \mathbf{R}_{k,ave.} = \text{average}\left(\mathbf{R}_{k,inst.}\right) \tag{3.10}$$

where $\mathbf{R}_{k,inst.} \in \mathbb{R}^{M\times M}$ is the instant covariance matrix with non-negative elements, and $\mathbf{R}_{k,ave.}$ is the averaged (long-term) covariance matrix per PRB of $\mathbf{R}_{k,inst.}$ which is looped over antenna groups and UE transmitting antennas [37]. Both of the covariance matrices have non-negative eigenvalues.
Channel $\mathbf{H}$ or $\mathbf{H}_k$ is a vector Gaussian channel and it can be decomposed into a set of parallel, independent scalar sub-channels which are also Gaussian [38]. Since every linear transformation can be represented as a combination of the following three operations: a rotation operation ($\mathbf{U} \in \mathbb{C}^{R\times R}$), a scaling operation ($\mathbf{\Lambda} \in \mathbb{R}^{R\times M}$), and another rotation operation ($\mathbf{V} \in \mathbb{C}^{M\times M}$), we have

$$\mathbf{R}_{k,ave.} = \mathbf{V}_k \mathbf{\Lambda}_k \mathbf{\Lambda}_k^T \mathbf{V}_k^H, \text{ for } \mathbf{H}_k = \mathbf{U}_k \mathbf{\Lambda}_k \mathbf{V}_k^H \tag{3.11}$$

where, $\mathbf{\Lambda}_k$ is diagonal matrix of singular values calculated over UE k channel and can be written as $\mathbf{\Lambda}_k = \text{diag}(\sqrt{\lambda_1}, \sqrt{\lambda_2}, \ldots, \sqrt{\lambda_r})$ assuming that $\sqrt{\lambda_1} \geq \sqrt{\lambda_2} \geq \ldots \sqrt{\lambda_r}$, $\lambda_i \in \mathbb{R}$ is ith largest eigenvalue of the current UE channel matrix, and $\mathbf{U}_k$ and $\mathbf{V}_k$ are semi-unitary matrices so that $\mathbf{U}_k^H \mathbf{U}_k = \mathbf{I}_R$ and $\mathbf{V}_k^H \mathbf{V}_k = \mathbf{I}_M$. Unitary property also means that the columns of $\mathbf{U}_k$ and $\mathbf{V}_k$ are orthogonal.

The right-hand side semi-unitary matrix of $\mathbf{V}_k$ for UE k can be formed as

$$\mathbf{V}_k = [\mathbf{v}_{k1}, \mathbf{v}_{k2}, \dots]^T, \tag{3.12}$$

and beamforming weights for each UE is defined as

$$\mathbf{w}_i = \mathbf{v}_{i1}, \ i = 1, \dots, K\,. \tag{3.13}$$

As an example, magnitude of complex eigenvectors of $\mathbf{U}_k$ has been depicted in Fig. 3.4 in one of the simulation scenarios with 64 antennas at the BS side. As can be seen, columns can be chosen based on number of UE data transmission layers and since we already assumed 1 data layer per UE, only the first column is selected that also corresponds to the largest eigenvalue of the channel for that UE.

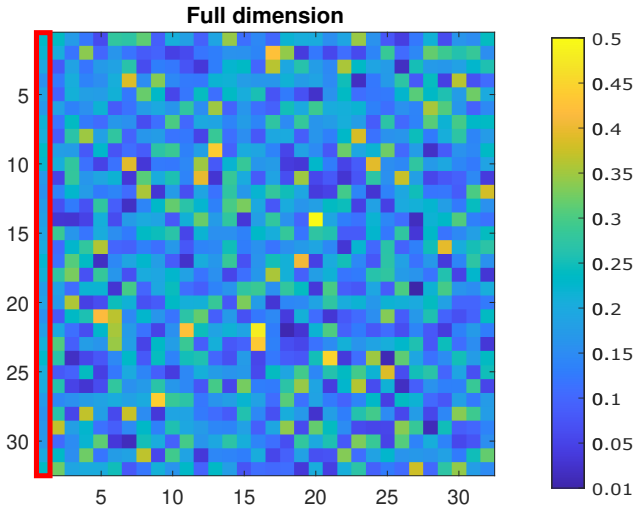

Figure 3.4. *First column of the channel eigenvectors in EZF method.*

By constructing the equivalent or effective channel matrix after obtaining right-hand side vectors of the channel matrix decomposition, we can calculate the precoding weights finally. Moreover, the equivalent channel of $\mathbf{H}_{eq}$ is defined as

$$\mathbf{H}_{eq} = (\mathbf{v}_{11}, \mathbf{v}_{21}, \dots, \mathbf{v}_{K1})^H \tag{3.14}$$

Channel knowledge is typically assumed at the receiver for the coherent combining. Therefore, diversity gain depends on the $\mathbf{H}$ availability at the transmitter. When $\mathbf{H}$ matrix is known to the transmitter, received SNR is optimized by using precoding and receiver weights matrices according to $\mathbf{V}$ and $\mathbf{U}$ matrices respectively.

By trying to decompose the channel matrix and using MRC coefficients for receiver

weights in Eq. 3.14, right hand side would be re-written as

$$\hat{\mathbf{s}}_k = \mathbf{v}_{k1}^H \mathbf{V}_k \mathbf{\Lambda}_k \mathbf{\Lambda}_k^T \mathbf{V}_k^H \mathbf{w}_k \, \mathbf{s}_k + \sum_{i=1,\, i\neq k}^{K} \mathbf{v}_{k1}^H \, \mathbf{V}_k \mathbf{\Lambda}_k \mathbf{\Lambda}_k^T \mathbf{V}_k^H \mathbf{w}_i \mathbf{s}_i \; + \mathbf{w}_k^H \mathbf{H}_k^H \mathbf{n}_k, \tag{3.15}$$

in which the first term would be the dominant term as

$$\left(\mathbf{v}_{k1}^H \mathbf{v}_{k1}, \mathbf{v}_{k1}^H \mathbf{v}_{k2}, \dots\right) \begin{bmatrix} \lambda_1 & 0 & \dots \\ 0 & \lambda_2 & \\ \vdots & & \ddots \end{bmatrix} \begin{pmatrix} \mathbf{v}_{k1}^H \mathbf{w}_k \\ \mathbf{v}_{k2}^H \mathbf{w}_k \\ \vdots \\ \mathbf{v}_{kr}^H \mathbf{w}_k \end{pmatrix} \mathbf{s}_k = (\lambda_1, 0, \dots, 0) \begin{pmatrix} \mathbf{v}_{k1}^H \mathbf{v}_{k1} \\ \mathbf{v}_{k2}^H \mathbf{v}_{k1} \\ \vdots \\ \mathbf{v}_{kr}^H \mathbf{v}_{k1} \end{pmatrix} \mathbf{s}_k = \lambda_1 \mathbf{s}_k, \tag{3.16}$$

where λ_1 is the biggest eigenvalue of the effective channel matrix corresponding to the first sorted eigenvector of UE k.

Furthermore, the second term in Eq. 3.15 results in zero for $k \neq i$ due to the orthogonality of ZF step on different UEs beamforming weights, and can be expressed as

$$\sum_{i=1,\, i\neq k}^{K} \mathbf{v}_{k1}^H \, \mathbf{V}_k \mathbf{\Lambda}_k \mathbf{\Lambda}_k^T \begin{pmatrix} \mathbf{v}_{k1}^H \mathbf{v}_{i1} \\ \mathbf{v}_{k2}^H \mathbf{v}_{i1} \\ \vdots \\ \mathbf{v}_{kr}^H \mathbf{v}_{i1} \end{pmatrix} \mathbf{s}_i = 0 \,; \;\; \mathbf{v}_{kr}^H \mathbf{v}_{i1} = 0 \; \forall i \neq k. \tag{3.17}$$

Final expression for $\hat{\mathbf{s}}_k$ would be

$$\hat{\mathbf{s}}_k = \lambda_1 \mathbf{s}_k + \mathbf{v}_{k1}^H \mathbf{H}_k^H \mathbf{n}_k. \tag{3.18}$$

After channel decomposition, it can be seen that subchannels with better condition have larger eigenvalues. According to the water-filling power allocation and the way it interprets channel capacity in equation 3.5, large eigenvalues increase the capacity, such that more power is transmitted towards the better subchannel between each UE and the BS [14].

3.3 A less computation-intensive eigen-based zero-forcing (LC EZF)

In addition to the normal EZF beamforming method, a less computation-wise method is introduced which offers reduced complexity in SVD calculations. This method saves complex data matrix operations comparing to EZF method and in section 4.3.1 we can see related simulations output for all of the scenarios.

The detailed technical description of the considered LC EZF method is omitted from this thesis due to its confidential nature. However, based on the considered simulation scenarios and the followed numerical results, described in chapters 4 and 5, respectively, it is clear that the LC EZF method can offer a highly competitive practical solution for EZF beamforming scenarios.

4 SIMULATION SCENARIOS

In this thesis work, Nokia internal link-level simulation environment is used to run 5G NR downlink scenario simulations. This environment is synced up with the latest 3GPP releases 15 and 16. In order to run a simulation, an script file should be created containing all the necessary parameters of the desired scenario including gNb, UE's, and the physical channels in between.

4.1 Simulation environment

Necessary FXP or FLP switches should be selected based on the specific system intellectual properties (IP) we intend to be taken part in our simulation. In the implemented beamforming algorithms, there are some manual FXP switches shown in gray color in table 4.1 to compare the performance loss over several permutations. Some of the system parameters which remain unchanged during all the scenarios are the followings:

- Carrier frequency : 3500 MHz
- Bandwidth : 20 MHz
- Duplex mode : TDD
- PDCCH and SRS symbols location: [1, 2] and [13]
- PDSCH allocated data symbols : [4, 5, 6, ..., 12]
- RF beamforming : disabled
- BTS antenna array : uniform linear array (ULA)
- Channel type: 3GPP 3D model
- Noise power : -45 dB to +10 dB

Each FLP scenario is compared to a FXP scenario, which his called a reference scenario, so that the graphs reflects the differences of changing one specific parameter at a time. The reference scenario is configured in Table 4.1 below.

UEs are configured with the following settings:

- Velocity : 3 Km/h
- Decoder : MMSE
- Antenna slant type: vertical, horizontal
- Channel estimation type : real (based on received signal including noise)

Table 4.1. *Default parameters of the reference scenarios. Parameters marked with * are fixed in all scenarios.*

parameters	values
SCS (KHz)	30
Channel bandwidth (MHz) *	20
MCS table *	2
MCS index	21
Beamforming method	LC
IFFT model	FXP
SVD+covariance matrix model	FXP
Weight calculation model	FXP
UEs directions (degree)	0,40
Number of UEs *	2
UE antenna number	2x2
BTS antenna number	16

- RF beamforming : disabled
- Reference signals : SSS (no PBCH DMRS)
- UE antenna array : uniform rectangular array (URA)

Simulations are using MCS 21 (8-QAM modulation and 0.694 coding rate) so that the expected performance loss between FLP and FXP is better depicted and more noticeable.

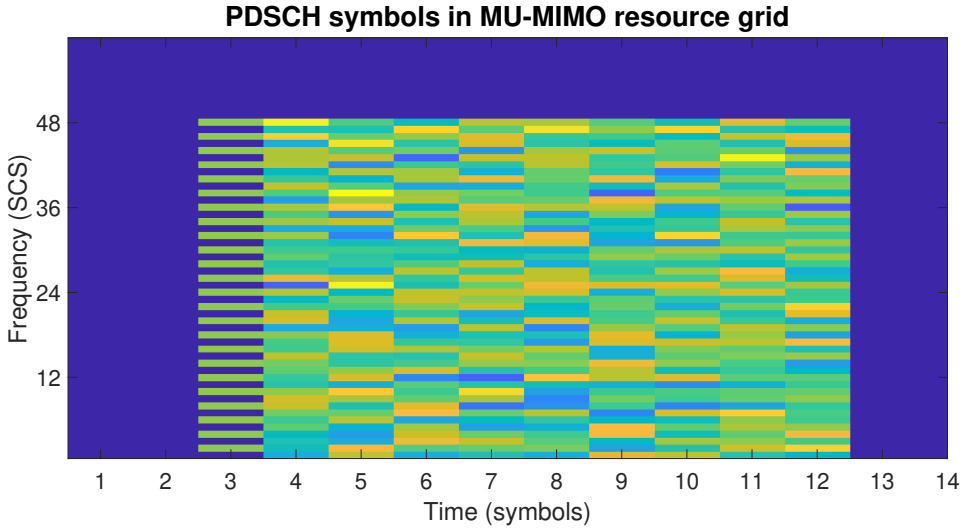

Figure 4.1. *PDSCH symbols for all UE's added on top of each other after beamforming. DMRS symbols are located at symbol 3. Different colors come from different magnitude of OFDM symbols of the same location which are generated randomly for each UE.*

When simulation is done for the given simulation length, results are dumped into a file so that they can be extracted later for post processing purposes, namely plotting. Output data includes raw data bit error rate, block error rate, post combining SINR at the receiver,

system throughput, noise power, and signal power.

4.2 Studied data formats

Data in terms of bits, as shown in Fig. 4.2, is represented in two's complement format by an integer part (exponent) and a fractional part (mantissa), respectively specified with m and n number of bits, and 1 bit for the data sign [22]. According to IEEE standard for floating-point arithmetic (IEEE 754), a floating-point data has 8 bits and 23 bits reserved for the integer and fractional parts respectively that is 32 bits in total, or 64 total number of bits in case of double precision format.

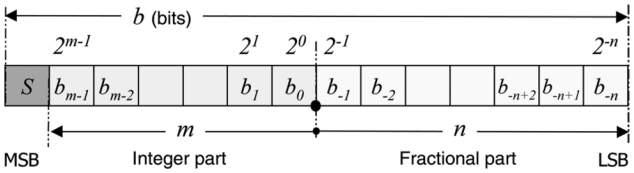

Figure 4.2. *Floating point accuracy*

Data dynamic range is obtained by number of bits required for the integer part to avoid overflowing and determines which extreme values to be represented. The data word length $(1 + m + n)$ in fixed-point format is a trade-off between implementation efficiency and computational accuracy, so that the chip area is minimized as long as data accuracy constraint is met.

In order to convert I and Q data into the desired FXP data type, a quantization function is used so that it takes care of both real and imaginary parts of the data. As depicted in Fig. 4.3, there are several input options for this generic function as followings: quantization types (floor, round, ceil, truncation, round to $\pm\infty$), saturation types (normal, symmetric), sign bit, integer bits number, and fractional part bits number.

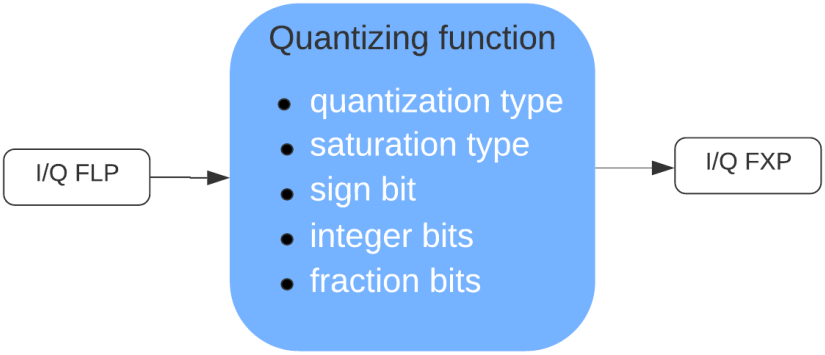

Figure 4.3. *Quantizing function parameters*

Here in the scenarios several input arguments will be used, namely different number of fraction bits and types of quantization. Quantizing function is deployed at the beginning and at the end of each block, such that input and output I/Q data of a certain block are affected by this data format. This way, data format is applied twice to ensure the data accuracy within each block.

Followings are used as inputs for quantization function and data range will be $\left[-1+2^{-15}, 1\right]$ with steps of $2^{-15} = 0.00003051757$:

- Quantization type: round
- Saturation type: asymmetric
- Sign bit: 1
- Integer bit: 0
- Fraction bits: 15

Quantizing function is used only within beamforming function and other parts of the downlink baseband processing are kept as floating-point.

4.3 Complexity and performance: FXP vs. FLP

Beamforming block is comprised of 4 different blocks as shown in Fig. 2.8. LC method can reduce the complexity in EVD or SVD calculations for up to 3 times comparing to the normal EZF method. Despite of the reduced complexity of SVD in LC EZF method, chapter 5 indicates that performance is almost same as in EZF. SVD outputs the channel eigenvectors which are an elemental part of eigen-based beamforming.

Scenarios are compared to two reference simulation for both EZF and LC EZF. Since MCS 4 has very small BER values for some scenarios, there is 0 value for BER at high SNRs and nothing can be interpreted out of the zeros. First solution would be to increase simulation length. Using 400ms for simulation length, each run took around 2.5 days to sweep over 56 different SNR values, and longer simulation length is not applicable due to limited time of this thesis work. Also, as a good trade off after trying some other MCS values, MCS 21 is preferred so that non-zero output values will be used for comparison purposes. Table 4.3 shows all of the MCS values and our preferred MCS indices are highlighted.

Transmitting signal and noise power varies according to the simulation environment configurations and scenario parameters. To maintain a fair comparison at the same SNR range, SNR values have to be interpolated to integer values. This range may differ from one scenario to another, however in one certain scenario all models of EZF and LC EZF methods share a same SNR range.

4.3.1 Scenarios

Every scenario is based on only one parameter variation for both beamforming methods, and scenarios are simulated using FXP and FLP models. The scenario MCS 4 is an exception in which two parameters are changed. Parameters that were modified are listed in the table 4.2 and scenario names are reflecting the modified parameter.

Table 4.2. *Parameters of interest to be changed in the simulations. *In MSC 4 scenario, 15KHz SCS is used.*

#	parameters	scenario values	default values
1	Number of PRB	10	4
2	UE antenna	2TX 4RX	2TX 2RX
3*	MCS index	4	21
4	SCS (KHz)	15	30
5	Polarization projection	Enabled	Disabled
6	UE directions (degree)	30,40	0,40
7	BTS antennas	64 TRX	16 TRX
8	SVD calculation	Power iterative	Ideal

One of the underlying parameters that easily comes into mind regarding simulating a digital transmission is the MCS index. 3GPP TS 38.101-1 version 15.3.0 document provides some downlink scenarios suggestions using MCS indices in appendix A3.3 but in this investigation only MCS 4 is selected to study data format impact and LC EZF method, due to simulation time limits mentioned earlier. This scenario is the only exception which has two parameter changes at once, with 15KHz SCS as the second modified parameter. However, simulations results for both 15KHz and 30KHz SCS are added to section 5.

Overall channel correlation and independent subchannels are linked to the number of antennas at both BS and UE sides. As the consequence, BTS antennas number is changed to 64TRX stands for 64 transceiving antennas, as well as UE antenna configuration is changed to 2T4R which means 4 receiving and 2 transmitting antennas are used.

Subcarrier spacing is changed from 30KHz to 15KHz to see how frequency allocation size would be influencing the models. Higher SCS sizes including 60KHz requires to change the carrier frequency which results in changing two parameters in one scenario at once, and therefore higher SCS's are skipped for this thesis work.

Another mean to study frequency effects is to harvest physical resource block (PRB) allocation size. Default number of PRB is set to 4 or similarly 48 subcarriers as shown in Fig. 4.1 and it's increased to 10 PRBs in one scenario.

Vertical and horizontal polarizations are used in BTS antenna array and the simulator is configurable with a polarization projection switch. This features enables the simulation to

Table 4.3. *MCS index table 2 for PDSCH: table 5.1.3.1-2 from 3GPP TS 38.214 version 15.2.0.*

MCS Index I_{MCS}	Modulation Order Q_m	Target Code Rate R $\times$ [1024]	Spectral Efficiency (bit/sec/Hz)
0	2	120	0.2344
1	2	193	0.377
2	2	308	0.6016
3	2	449	0.877
4	2	602	1.1758
5	4	378	1.4766
6	4	434	1.6953
7	4	490	1.9141
8	4	553	2.1602
9	4	616	2.4063
10	4	658	2.5703
11	6	466	2.7305
12	6	517	3.0293
13	6	567	3.3223
14	6	616	3.6094
15	6	666	3.9023
16	6	719	4.2129
17	6	772	4.5234
18	6	822	4.8164
19	6	873	5.1152
20	8	682.5	5.332
21	8	711	5.5547
22	8	754	5.8906
23	8	797	6.2266
24	8	841	6.5703
25	8	885	6.9141
26	8	916.5	7.1602
27	8	948	7.4063

apply beamforming weights projection on channel estimation followed by a normalization step. Projection of both polarization steering vectors on user-specific channel estimation and covariance matrix can be used to reduce the covariance matrix estimation errors [6]. This projection switch is enabled in one scenario and observations are listed in the results section.

Where more than one UE is using same spatial channel model, they need to be differentiated in direction of arrival (DoA) angle from the BS. Reference cases use 0 and 40

degree and we are testing 30 and 40 degrees to see how interference affects the system performance.

SVD block is required to calculate the dominant eigenvector of the channel correlation matrix. In the above scenarios, Matlab's built-in svd-function is responsible for this decomposition. A new scenario substitutes this Matlab built-in function with a power iterative SVD calculation method for square matrices, also called power method [16]. Channel correlation matrix and number of iterations are inputs to the power iterative method and the amplitude of eigenvalues should be non-identical to make sure of convergence:

$$|\lambda_1| > |\lambda_i|\,, \;\; i = 2, ..., n. \tag{4.1}$$

5 RESULTS

This section visualizes the performance loss in terms of how much FXP acts worse comparing to its FLP counterpart. It can be also seen that some simulated scenarios performs better than the reference cases, however references dominated the comparison in several scenarios as it was expected.

Bit error rate (BER) is the average number of erroneous bits occurring in a given number of bit transmissions which is usually expressed as a ratio [9]. Raw data BER here stands for non-decoded receiving downlink signals. SINR or signal-to-interference-plus-noise ratio is another expressions in MIMO communications which considers channel noise, as well as the interference coming from other UEs compared to the received signal power of a desired UE.

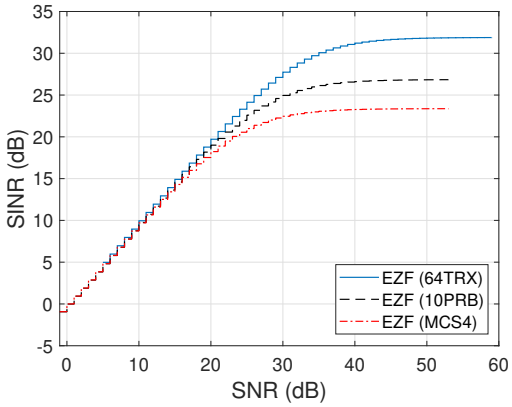

Figure 5.1. *Converging pattern of SINR in FLP models.*

Due to the presence of multiple UEs in a MU-MIMO DL channel, there would always be interference in real life scenarios, regardless of how good the channel's condition is. This fact is transparent in BER graphs, so that from a certain SNR value onward, BER starts to converge with pretty small fluctuations around that convergence value. Fig. 5.1 shows this converging pattern for SINR in a similar manner.

Green arrows in Fig. 5.2 and Fig. 5.3 are pointing to better performance of reference scenarios and FLP models respectively. Raw data BER graph tells us about the FLP model performance of parameter-varying test cases and references for all SNR values. References are similar for all cases and plotted with ticker markers. ΔBER graph is simply the BER subtraction of reference from their corresponding scenarios, in which higher values results in better reference BER performance or in other words, degraded

performance of that scenario.

5.1 Scenario 1: 10 PRBs

Since the beamforming module takes all reference signals of those 10 PRBs together into account to create beamforming weights, then system performance will be affected. In this case, channel estimation resolution in frequency axis is reduced and as a result SINR and BER outcomes are degraded through both FXP and FLP models.

According to Fig. 5.2 and 5.3, the reference case with 4 PRBs performs better than 10 PRBs by 5×10^{-4} on average with respect to BER graph. FLP model also outperforms FXP model at almost all SNR values, close to references for BER and worse than references up to 5×10^{-3} dB for SINR curves .

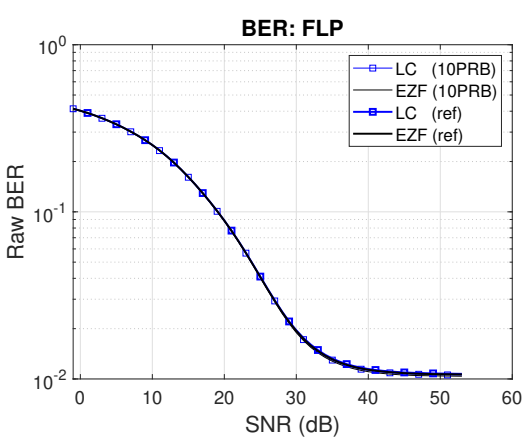

(a) *Raw data BER of FLP models.*

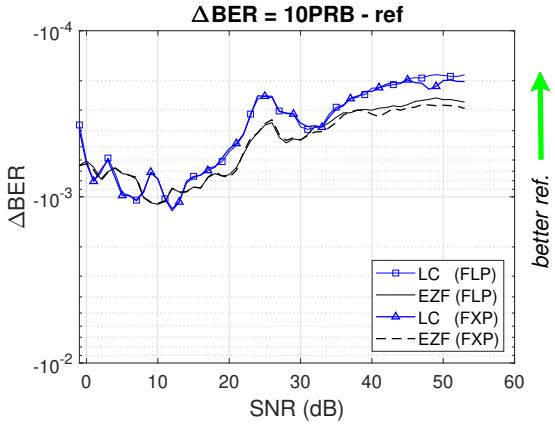

(b) *Differences of FLP and FXP models for 10 PRBs allocation against references.*

Figure 5.2. *10 PRB size scenario vs. reference scenarios: performance differences ($\Delta BER = BER_{scenario} - BER_{reference}$)*

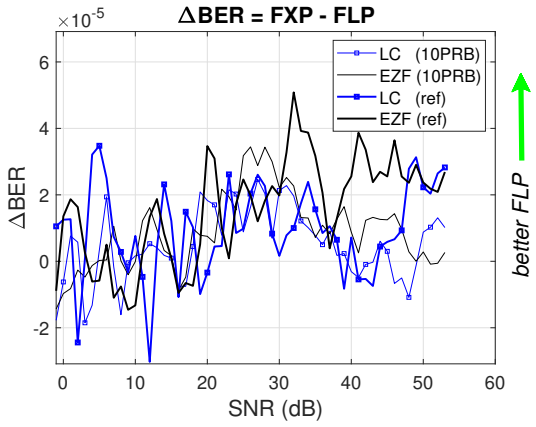

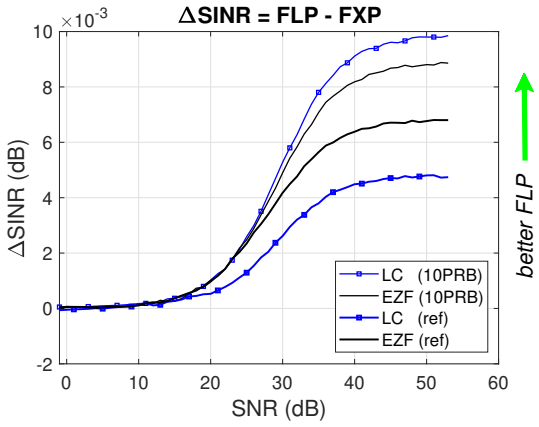

Figure 5.3. *Impact of data format on PRB allocation size, which is derived from difference between FXP and FLP. ($\Delta BER = BER_{FXP} - BER_{FLP}$, $\Delta SINR = SINR_{FLP} - SINR_{FXP}$)*

5.2 Scenario 2: 2T4R

Increased number of receiving antennas at the UE side makes the downlink subchannels less correlated to each other and contains smaller interference. Additionally, more receiving antennas helps to exploit receiving diversity and spatial multiplexing.

BER performance is improved in the 2T4R scenario compared to the references as shown in Fig. 5.4. BER improvement is higher at low SNR range from 0 to 20 dB. At this SNR range the BER improvement is nearly 0.14, but it starts to decrease exponentially for higher than 20 dB SNR values, stopping at 10^{-5}. There are some fluctuation after SNR 50 dB indicating that FXP model of EZF has worst performance among all of them.

While other cases are performing in our favour after the data format impact in Fig. 5.5, EZF FXP model behaves strangely and is performing better than FLP model by 1.5×10^{-5} in BER and roughly 0.08 dB in SINR. This pattern peaks at 10 dB SNR and it joins the other plots oscillating around 0 in BER graph and for SINR graph, it rests above 0 meaning that after 40 dB SNR FLP model acts better than FXP.

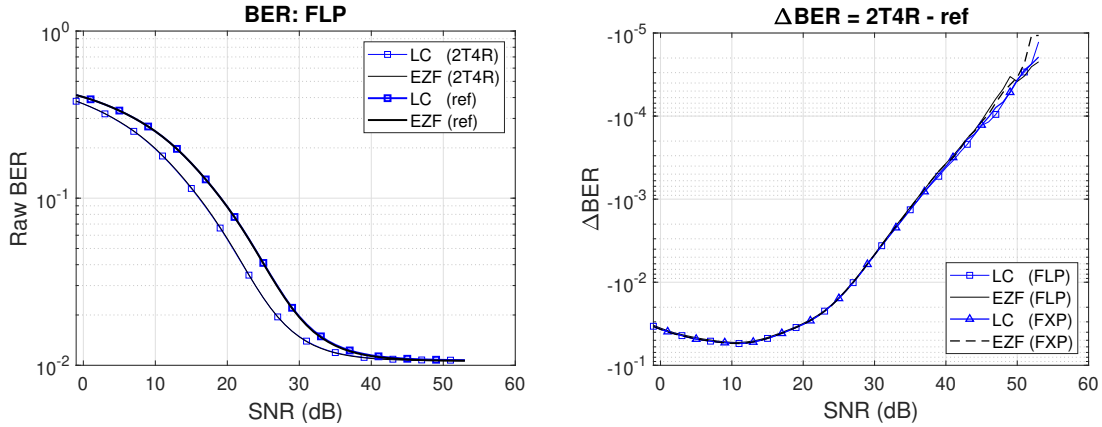

Figure 5.4. *2x4 UE antennas scenario: FLP and FXP differences against reference.*

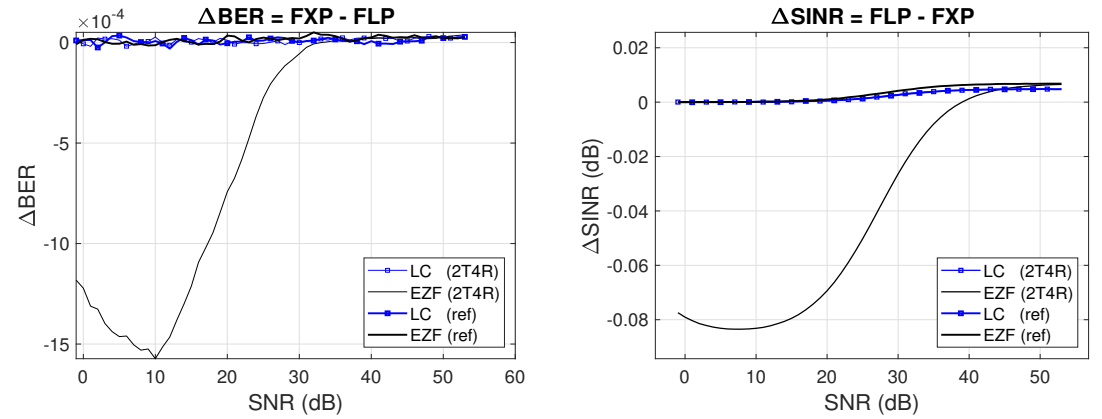

Figure 5.5. *Data format impact on UE antennas.*

5.3 Scenario 3: MCS 4

Switching from MCS 21 to MCS 4 with 30KHz SCS applies a huge gap from corresponding 30KHz reference scenarios in the BER figure 5.6, providing a maximum of 100 times better BER and roughly 10 times better BER for large SNR values. ΔBER contains only negative values, meaning that MCS 4 scenario has better BER values for both EZF and LC EZF methods, FLP and FXP models.

Data format impacts BER data to flicker around 0 with an amplitude of 10^{-5}dB, however SINR reaches 4×10^{-3} steadily. In Fig. 5.7, SINR plots stay above zero, placed close to each other, and therefore, FLP model has higher values than FXP model over the entire SNR range.

Performance results in case of using 30KHz SCS is plotted using dotted line and it drastically goes below 10^{-6} BER.

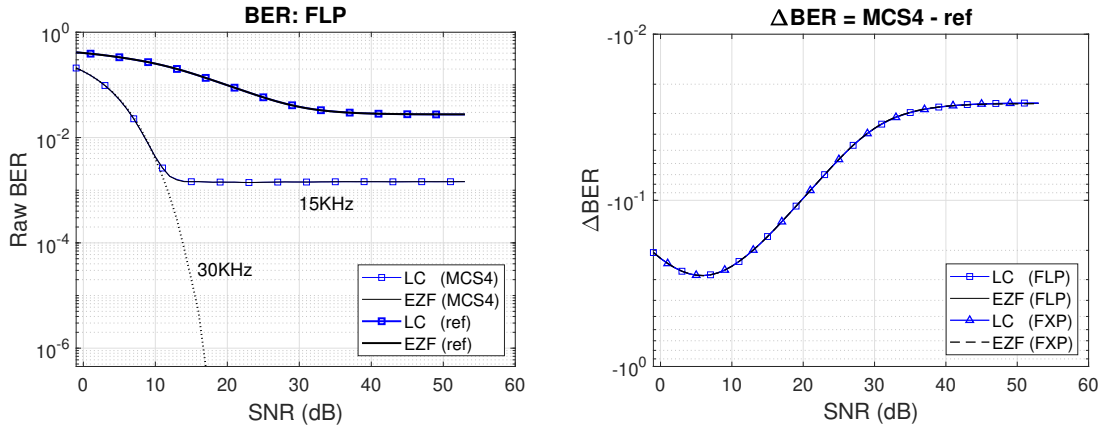

Figure 5.6. *MCS 4 scenario: FLP and FXP model performance against reference scenarios.*

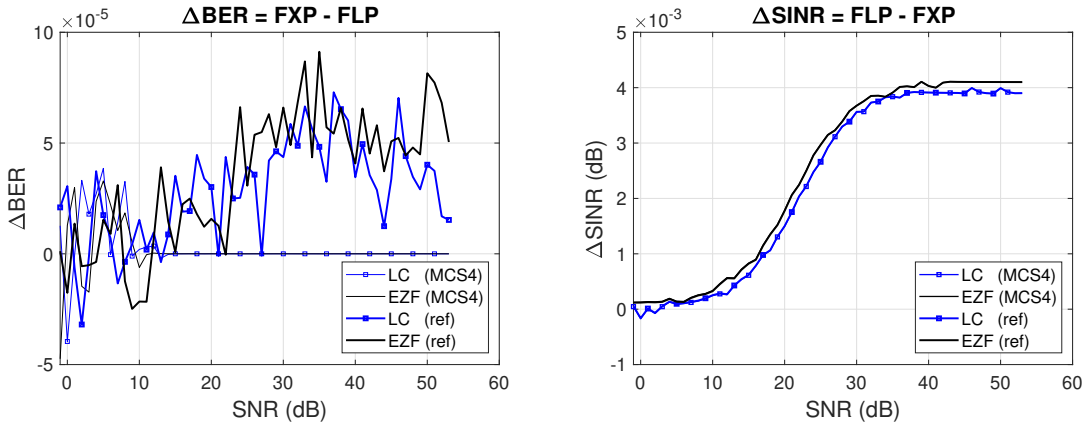

Figure 5.7. *Data format impact on MCS index.*

5.4 Scenario 4: SCS 15KHz

User data bandwidth consists of sinc waves in frequency domain and it's calculated as a multiple of subcarrier spacing size. Choosing a smaller SCS, therefore, reduces the effective bandwidth and the throughput as can be seen from Fig. 5.8 and 5.9.

In BER graph it's evident that 15KHz SCS has undesirable performance over 30KHz SCS of reference cases, and this differences is nearly 0.11 for large SNRs.

Both beamforming methods deliver worse FXP performance comparing to reference scenarios as expected and data format is affecting them more than it does to references. SINR graph indicates that 15KHz case has more similar SINR than references, especially regarding the EZF reference.

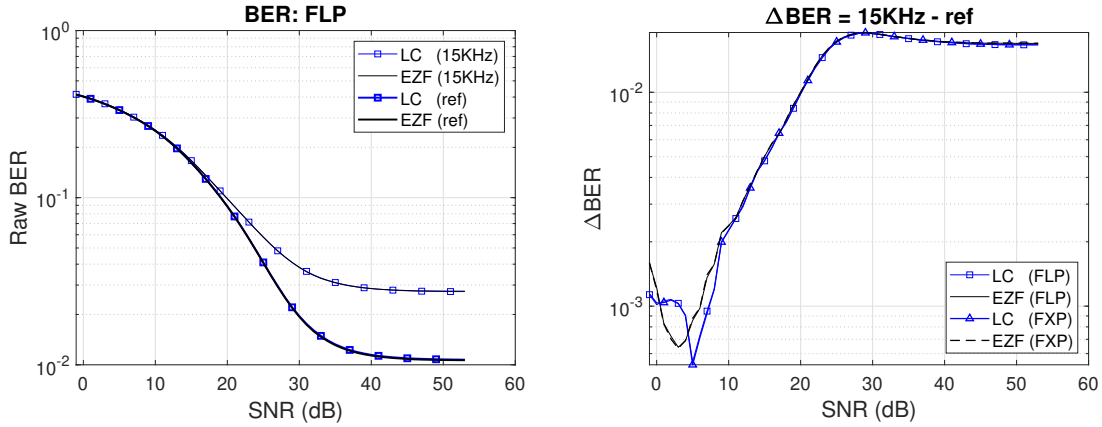

Figure 5.8. *15KHz SCS scenario: FLP and FXP model differences compared to reference scenarios.*

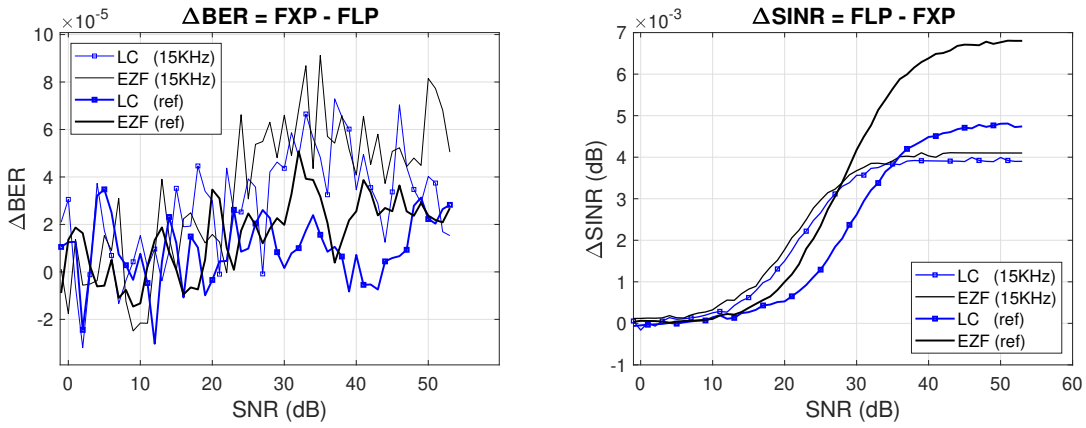

Figure 5.9. *Data format impact on subcarrier spacing size.*

5.5 Scenario 5: Polarization projection enabled

Projection of the beamforming weight vector on estimated channel covariance shows that reference scenarios without projection perform better under the channel model used in the simulation.

As shown in Fig. 5.10, BER performance in both models of EZF method is closer to the reference cases than LC EZF method and this statement is valid for SNR values larger than 34 dB. Largest gap takes place at 12 dB SNR with 4×10^{-3} distance from the reference scenarios.

Data format impact on BER graph has almost same range as the FLP model with an average of 3×10^{-5} gap. SINR difference after applying data format is not far from reference scenarios according to Fig. 5.11. However, FXP model for both methods acts better than FLP until roughly 30 dB SNR and then this patter reverses on favour of FLP model, performing better than references by maximum of 10^{-3} dB deviation.

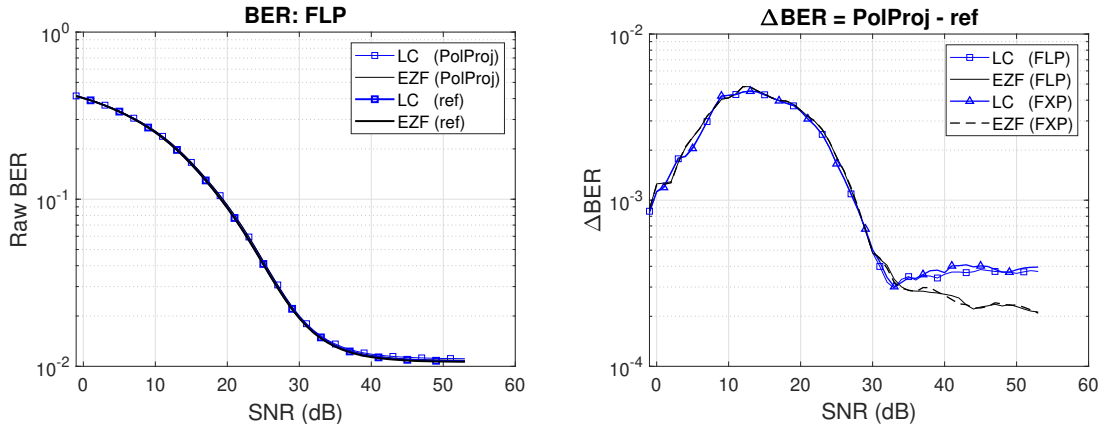

Figure 5.10. *Polarization projection enabled scenario: FLP and FXP model differences against reference scenarios.*

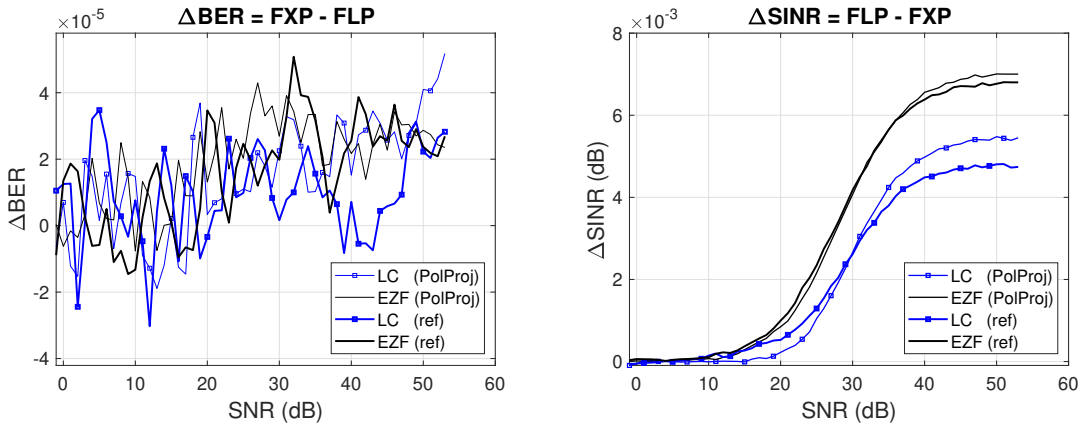

Figure 5.11. *Impact of data format on polarization projection.*

5.6 Scenario 6: UE 30,40

Closer direction of arrival angles for different UEs significantly reduces the system performance. As shown in Fig. 5.12, BER curves of the new scenario are lying far from reference scenarios and this decreasing pattern becomes stronger with increasing SNR value. Reference BER performance beats this scenario by almost 0.1 difference which is the largest gap comparing to other scenarios. It has an exponential behaviour from low SNRs until 25 dB and then starts to converge.

Data format is again impacting this scenario and we can see the similar pattern in comparing with the references and FLP wins the comparison by roughly 20 times better performance. Fig. 5.13 indicates that SINR is not an exception and again it has the largest gap between FLP and FXP models in this scenario. Surprisingly, LC method has less FXP-FLP difference than EZF method, with final difference points of 0.063 dB and 0.055 dB for EZF and LC EZF respectively.

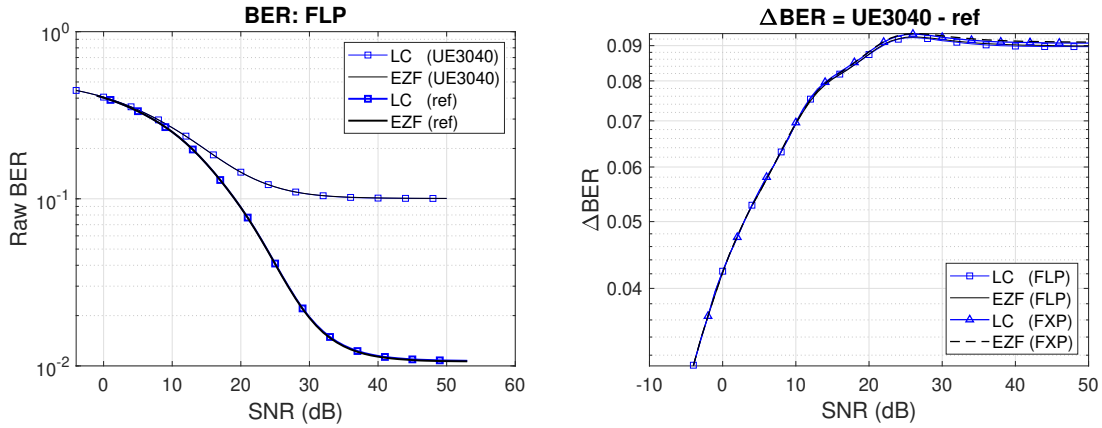

Figure 5.12. *UE angles 30,40: FLP and FXP model differences against references.*

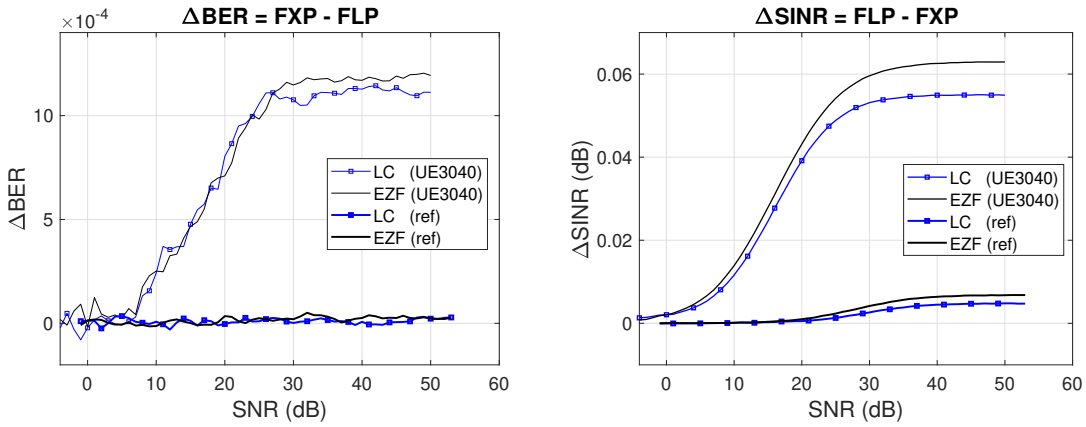

Figure 5.13. *Data format impact on UE directions.*

5.7 Scenario 7: 64TRX

Spatial multiplexing and diversity are improved once more by applying larger antenna array size for the BS and we expect this modification to enhance the system performance. As it is clearly depicted in Fig. 5.14, there is a huge boost in BER performance especially at large SNR values and EZF performed better than LC EZF, having 4×10^{-4} value after 50 dB SNR. Difference with the references are placed on top of each other meaning that FLP and FXP models in this scenario lose same performance for both beamforming methods.

Data format affects this scenario less than references and it's close to 0 difference between FLP and FXP models at large SNR values. SINR figure 5.15 is behaving unexpectedly since FXP performance seems to be more identical to FLP after 10 dB SNR, however this improvement is only 10^{-3} dB.

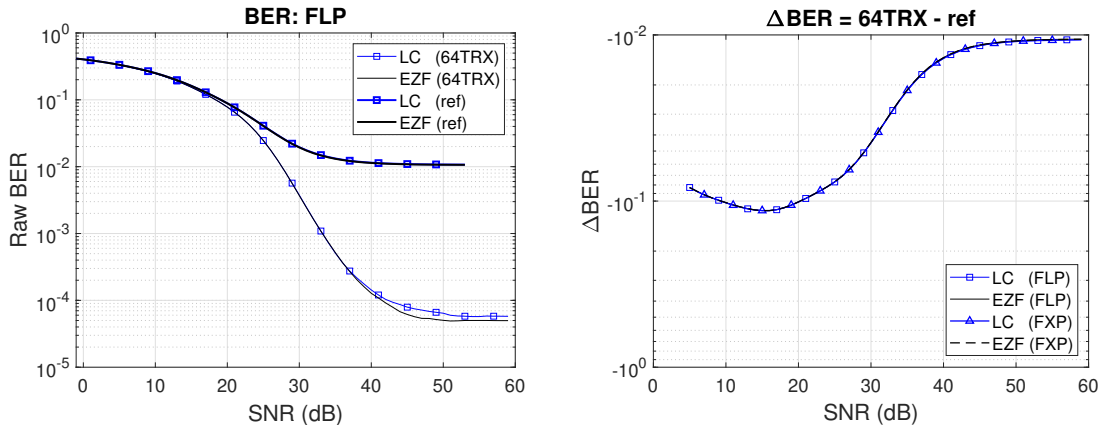

Figure 5.14. *64TRX BS antennas: FLP and FXP model differences against reference scenarios.*

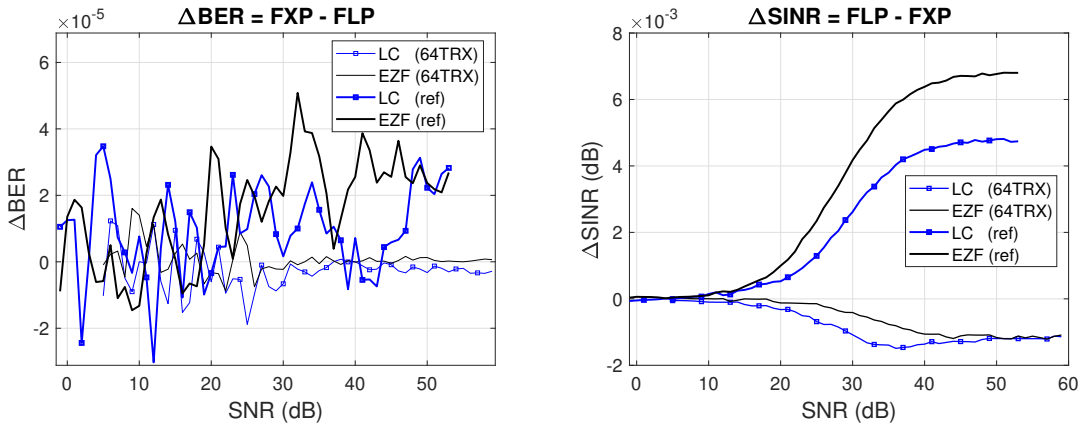

Figure 5.15. *Data format impact on BS antennas number.*

5.8 Scenario 8: Power method

Iterative power method in simulations almost overcame its possible issues, including enough number of iterations and eignevalue amplitude. BER performance tends to be in favour of references for several SNR values less than 30 dB. This difference toggles in the low SNR range between this scenario and reference cases, and after 30 dB, power method SVD results in reduced BER values of 2.5×10^{-4} approximately.

Applying data format to both beamforming methods shed light on almost similar loss as seen in references for ΔBER graph in Fig. 5.16. FLP model of normal EZF introduces SINR difference so that it performs better than FXP by roughly 10^{-3} dB. However, FXP model of LC EZF leads to better results for SNR less than 42 dB and at higher SNR it ends with higher SINR values for FXP model, as in Fig. 5.17.

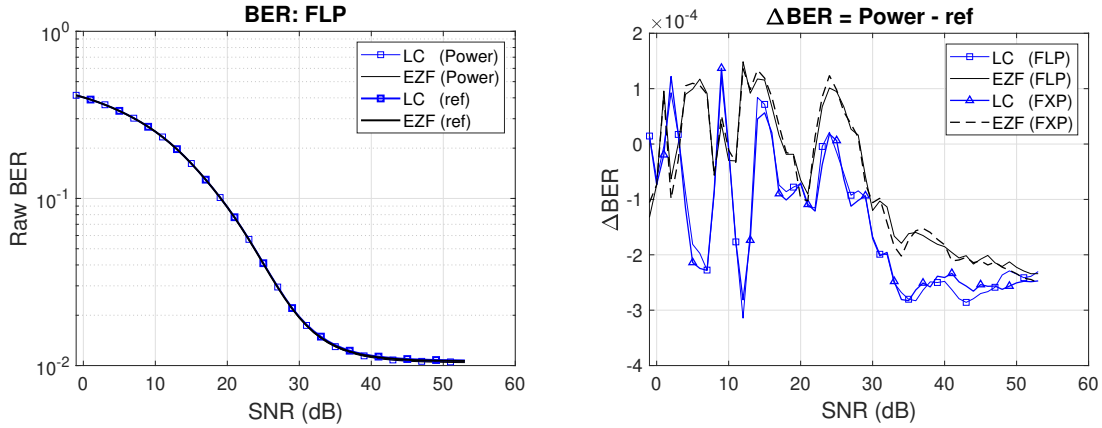

Figure 5.16. *SVD power method: FLP and FXP model differences of power method against references.*

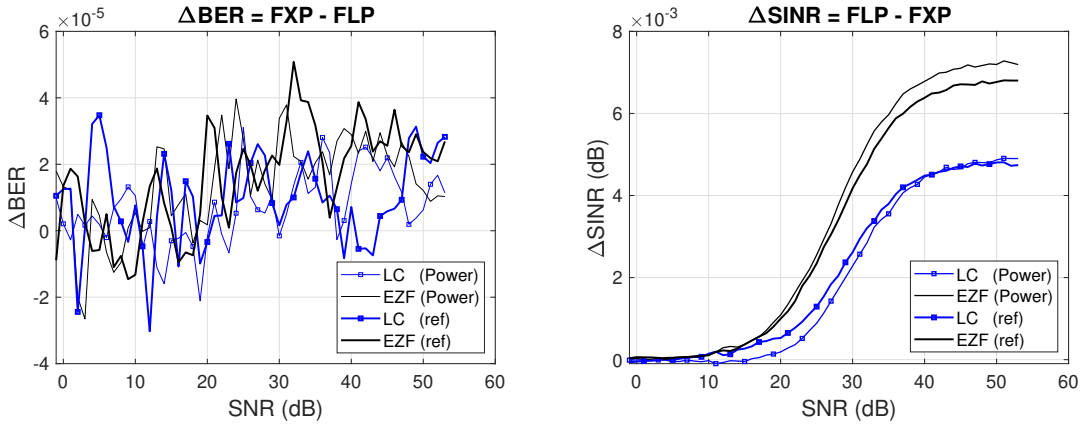

Figure 5.17. *Data format impact on SVD calculation method.*

5.9 Throughput

We noticed that throughput of FXP and FLP models are pretty similar and performance loss would be negligible with this data accuracy of 16 bits. To state it clearly, throughput of FXP and FLP models for larger PRB allocation size of 10 is shown in Fig. 5.18 and they perform similarly, same behaviour for two beamforming methods. The rest of scenarios follow the same trend and only FXP results are present.

Throughput is surged from 5.68 Mbps to 14.15 Mpbs in 10 PRB scenario in EZF method. EZF and LC EZF methods throughput oscillate around the breaking point of 30 dB SNR and EZF has higher data rate of 0.1 Mbps, while this gap reduces to 0.03 Mbps around 46 dB SNR.

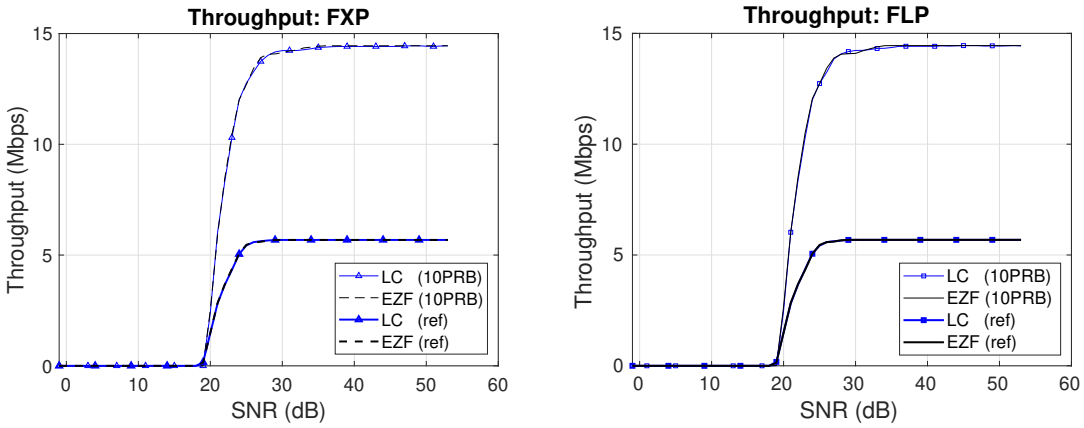

Figure 5.18. *Data rate for 10 downlink PRB, FXP and FLP models.*

64TRX and 2T4R scenarios achieved final values precisely same as references. As can be seen in Fig. 5.19, breaking point occurs at lower SNR values, 7 dB and 3 dB SNR earlier than references using 64TRX and 2T4R scenarios respectively. This gap remains for lower SNR values in 2T4R scenario until it converges to 0 Mbps at 15 dB SNR, however 64TRX scenario meets references already at 20 dB SNR.

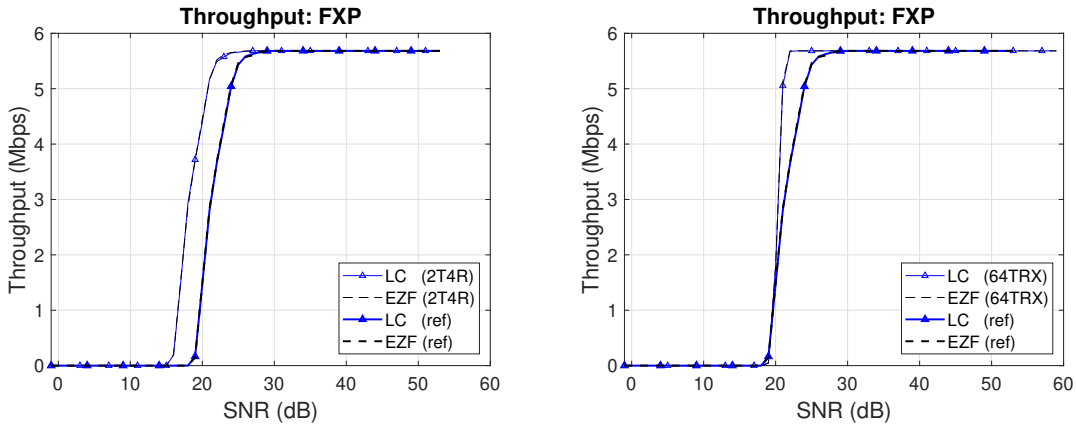

Figure 5.19. *2T4R and 64TRX scenarios throughput using FXP models.*

Fig. 5.20 tells us about MCS4 and UE3040 scenarios and how throughput performance is

dropped with these configurations. Lower MCS index with 15KHz SCS achieved UE data rate of 0.621 Mbps and this is valid for both EZF and LC EZF method, and the breaking point is located at 5 dB SNR. The reference cases using same subcarrier spacing size achieved 2.854 Mbps at high SNR range and this translates into 2.23 Mbps of differences. Same scenario in case of using 30KHz SCS approaches the maximum data rate of 1.238 Mbps and breaking point of 6 dB SNR.

Another performance degradation is observed from smaller angular space between UEs. This scenario, again, harmed system performance the most among other throughput results. 1.254 Mbps and 1.103 Mbps the highest data rates achieved by EZF and LC EZF respectively. Largest gap is found between LC EZF and references at 4.580 Mbps. LC EZF performs better until 32 dB SNR and at higher SNR onward EZF is preferred over LC EZF.

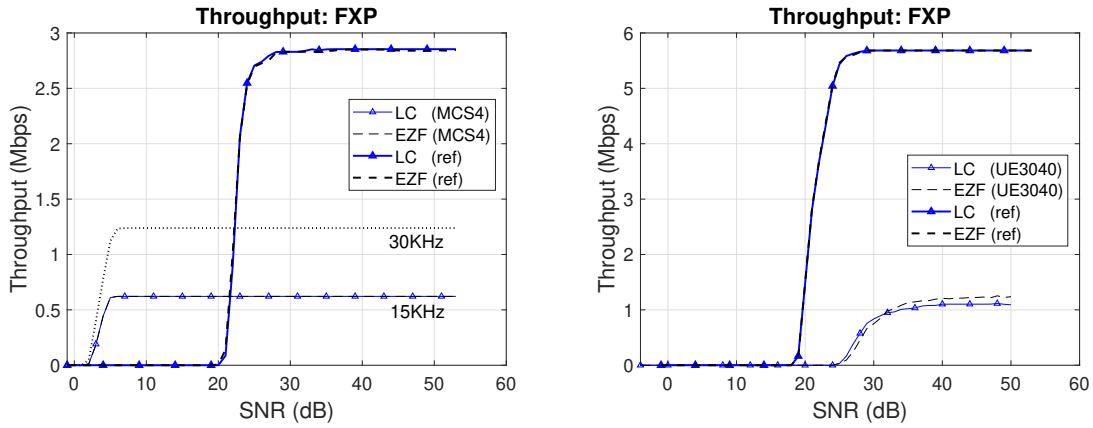

Figure 5.20. *MCS4 and UE3040 scenarios data rate difference.*

Two scenarios of polarization projection and power iteration have quite similar data rates as their references. Identical final throughputs are achieved from both, as shown in Fig. 5.21. The observed throughputs of 5.683 Mbps are similar with the reference scenarios results.

Polarization projection leads to lower data rate for SNR values less than 26 dB. The breaking point is observed at 27 dB SNR, and it reaches zero throughput almost 1 dB earlier than references.

Decreasing subcarrier spacing size to 15KHz directly affects the throughput, which drops by 50.14%. Moreover, the breaking points are shifted 1 dB earlier than references as shown in Fig. 5.22. LC EZF throughput is placed at the same or higher level than normal EZF, with 0.054 Mbps difference at 52 dB SNR.

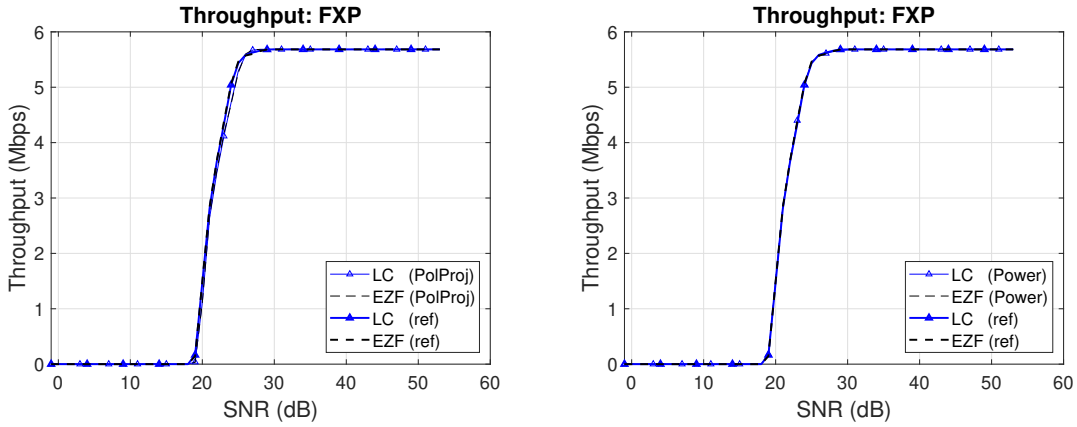

Figure 5.21. *Polarization projection and SVD power iteration method throughput after data format impact.*

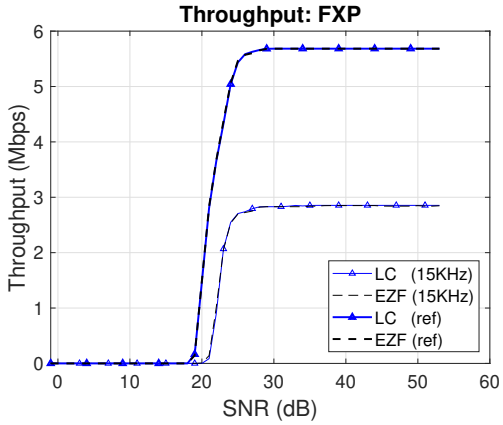

Figure 5.22. *15KHz SCS scenario data rate.*

5.10 Discussion and statistical observations

This section studies performance differences between FXP and FLP for all scenarios in one figure. Furthermore, studies on data format impact is statistically visualized through figures 5.23 and 5.24. Input values for these histogram plots are taken from results considered earlier, including ΔBER and ΔSINR results.

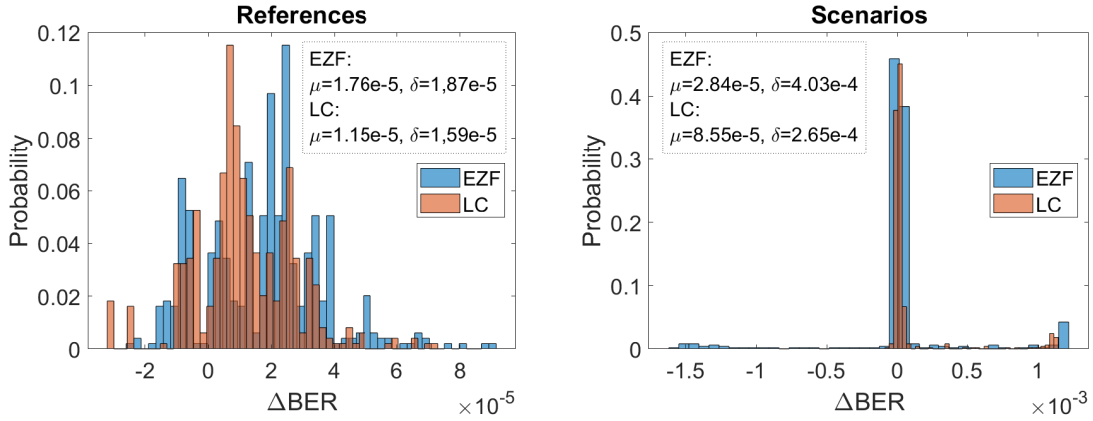

Figure 5.23. *Histogram of $\Delta BER = BER_{FLP} - BER_{FXP}$.*

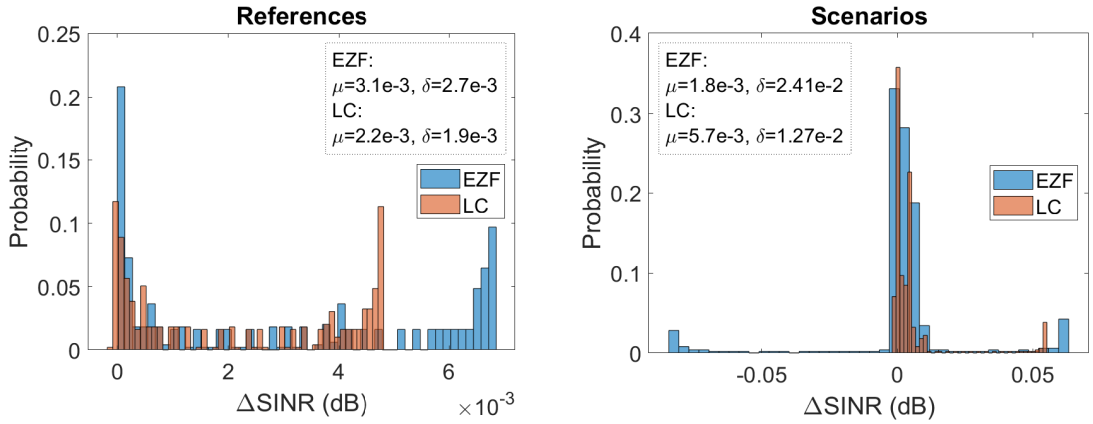

Figure 5.24. *Histogram of* $\Delta SINR = SINR_{FLP} - SINR_{FXP}$.

Reference FXP models have smaller BER deviations from their FLP reference comparing to test scenarios. LC EZF has smaller performance loss average and variance in terms of BER, however EZF performs more ideally than LC EZF in tested scenarios. Scenarios have larger averages and variances comparing to reference models, and EZF wins the data accuracy of test scenarios with almost 4 times smaller mean and variance.

ΔSINR is evenly impacted in reference cases and LC EZF similar to ΔBER performs better than normal EZF method. In tested scenarios performance loss is lower in EZF method in terms of both average and variance.

6 CONCLUSION

This thesis work studies the performance of 5G communication systems, especially the difference between fixed-point and floating-point models of digital downlink beamforming with eigen-based zero-forcing. This comparison of system performance is vital in industrial applications to have the outputs of system blocks aligned together in both models. Additionally, system performance loss of data format impact on reference model is investigated and changes are compared for several system parameters. System models and simulations are carried out within Nokia Networks resources. The thesis work, including the main objectives and framework, as well as the most essential research outcomes is summarized in Table 6.1.

Table 6.1. *Summary of this thesis work.*

Objectives	FXP modelling of two EZF beamforming methods and studying of data format impacts the performance in practical implementations.
Time frame	January 2020 - December 2020
Simulation environment	Matlab
Measurement units	BER, SINR, throughput
Transmission type	Downlink from BS, MU-MIMO fading channel
Major tradeoff	Extreme beamforming scenarios of a 5G downlink transmission require high precision for the precoding calculations. FLP computation is costly, whereas, FXP is simple but less accurate.
Outcomes	Performance loss due to FXP is less than 3% at extreme scenarios which is negligible, and it is worthy of data accuracy reduction and practical implementation feasibility.

Eight different scenarios were configured and simulated for both FXP and FLP models of EZF beamforming. Moreover, a less computation intensive EZF beamforming which is developed in Nokia simulators, so called LC EZF is studied. Scenarios are selected such that the differences are clearly notable. Performance is evaluated using SINR and BER parameters.

Fixed-point computation causes roughly 0.2% BER performance loss on average compared to the floating-point, whereas maximum difference is 3%. SINR also degrades 2.3% on average and peaks at 37% in one scenario. FXP model is accurate enough for

hardware implementation, especially when we consider all the benefits it offers. Differences between BER and SINR are practically negligible between studied beamforming methods, in the order of 10^{-5} for BER and 10^{-3} for SINR.

Expected output difference on FXP model simulations can be directly obtained from these analysis, such that 10^{-5} and 10^{-3} deviation in BER and SINR respectively doesn't harm the overall performance. Larger differences indicate either of inaccurate FXP modeling or invalid simulation configurations.

Possible future works includes considering user scheduling, simulating with larger number of users, and expanding using FXP model for other downlink modules in addition to beamforming. Additionally, Regularized EZF (REZF) beamforming and Iterative EZF (IEZF) beamforming can be studied in terms of FXP model performance. Regularized matrix inversion in REZF prevents poor performance when number of transmitting antennas is not much greater than number of served user equipments, or similarly ill-posed channel inversion scenario. IEZF has similar complexity as EZF but performs better in low and medium SNR scenarios, using some initial beamforming weights and converging approach.

REFERENCES

[1] 3GPP. *Study on New Radio (NR) access technology*. Technical Report (TR) 38.912. Version 15.0.0. 3rd Generation Partnership Project (3GPP), Sept. 2018.

[2] I. Ahmed, H. Khammari, A. Shahid, A. Musa, K. S. Kim, E. De Poorter and I. Moerman. A Survey on Hybrid Beamforming Techniques in 5G: Architecture and System Model Perspectives. *IEEE Communications Surveys Tutorials* 20.4 (2018), 3060–3097.

[3] N. Chiurtu, B. Rimoldi and E. Telatar. On the capacity of multi-antenna Gaussian channels. *IEEE International Symposium on Information Theory (IEEE Cat. No.01CH37252)*. 2001, 53.

[4] E. Dahlman, S. Parkvall and J. Sköld. Chapter 11 - Multi-Antenna Transmission. *5G NR: the Next Generation Wireless Access Technology*. Ed. by E. Dahlman, S. Parkvall and J. Sköld. Academic Press, 2018, 225–240. ISBN: 978-0-12-814323-0.

[5] N. Fatema, G. Hua, Y. Xiang, D. Peng and I. Natgunanathan. Massive MIMO Linear Precoding: A Survey. *IEEE Systems Journal* 12.4 (2018), 3920–3931. DOI: 10.1109/JSYST.2017.2776401.

[6] D. D. Feldman and L. J. Griffiths. A projection approach for robust adaptive beamforming. *IEEE Transactions on Signal Processing* 42.4 (1994), 867–876. DOI: 10.1109/78.285650.

[7] A. Flores, S. Quadri and E. Knightly. A Scalable Multi-User Uplink for Wi-Fi. (Mar. 2016).

[8] G. Frantz and R.Simar. *Comparing Fixed- and Floating-Point DSPs*. SPRY061. Texas Instruments. 2004. URL: https://www.ti.com/lit/wp/spry061/spry061.pdf.

[9] L. E. Frenzel. Chapter Sixty-Two - Testing Considerations. *Handbook of Serial Communications Interfaces*. Ed. by L. E. Frenzel. Oxford: Newnes, 2016, 229–232. ISBN: 978-0-12-800629-0.

[10] A. Goldsmith, S. A. Jafar, N. Jindal and S. Vishwanath. Capacity limits of MIMO channels. *IEEE Journal on Selected Areas in Communications* 21.5 (2003), 684–702.

[11] A. Goldsmith, S. A. Jafar, N. Jindal and S. Vishwanath. Capacity limits of MIMO channels. *IEEE Journal on Selected Areas in Communications* 21.5 (2003), 684–702.

[12] A. Goldsmith. *Wireless Communications*. Cambridge University Press, 2005. DOI: 10.1017/CBO9780511841224.

[13] T. Haustein, C. von Helmolt, E. Jorswieck, V. Jungnickel and V. Pohl. Performance of MIMO systems with channel inversion. *Vehicular Technology Conference. IEEE*

55th Vehicular Technology Conference. VTC Spring 2002 (Cat. No.02CH37367). Vol. 1. 2002, 35–39 vol.1.

[14] M. A. Khalighi, J. .-M. Brossier, G. V. Jourdain and K. Raoof. Water filling capacity of Rayleigh MIMO channels. *12th IEEE International Symposium on Personal, Indoor and Mobile Radio Communications. PIMRC 2001. Proc. (Cat. No.01TH8598)*. Vol. 1. 2001, A–A.

[15] N. Q. Khuong, N. Van Duc, N. Q. Trung and V. T. M. Tu. A precoding method for closed-loop MIMO-OFDM systems. *2008 International Conference on Advanced Technologies for Communications*. 2008, 431–433. DOI: 10.1109/ATC.2008.4760615.

[16] R. Larson and D. Falvo. *Elementary Linear Algebra, Enhanced Edition*. Cengage Learning, 2009. ISBN: 9781439044001. URL: https://books.google.fi/books?id=EGzCCAAAQBAJ.

[17] E. A. Lee. Programmable DSP architectures. I. *IEEE ASSP Magazine* 5.4 (1988), 4–19.

[18] L. Liu, J. Kuang and Z. Fei. Power Allocation for Eigen- Beamforming Used in Multi-Antenna System. *2007 IEEE 18th International Symposium on Personal, Indoor and Mobile Radio Communications*. 2007, 1–4.

[19] Lizhong Zheng and D. N. C. Tse. Diversity and multiplexing: a fundamental tradeoff in multiple-antenna channels. *IEEE Transactions on Information Theory* 49.5 (2003), 1073–1096.

[20] C. Luo, J. Ji, Q. Wang, X. Chen and P. Li. Channel State Information Prediction for 5G Wireless Communications: A Deep Learning Approach. *IEEE Transactions on Network Science and Engineering* 7.1 (Jan. 2020), 227–236. ISSN: 2327-4697. DOI: 10.1109/TNSE.2018.2848960.

[21] P. Marsch, Ö. Bulakci, O. Queseth and M. Boldi. Antenna, PHY and MAC Design. *5G System Design: Architectural and Functional Considerations and Long Term Research*. 2018, 263–313.

[22] D. Menard, R. Rocher and O. Sentieys. Analytical Fixed-Point Accuracy Evaluation in Linear Time-Invariant Systems. *IEEE Transactions on Circuits and Systems I: Regular Papers* 55.10 (2008), 3197–3208.

[23] C. B. Peel, B. M. Hochwald and A. L. Swindlehurst. A vector-perturbation technique for near-capacity multiantenna multiuser communication-part I: channel inversion and regularization. *IEEE Transactions on Communications* 53.1 (2005), 195–202.

[24] S. B. Purnapatra, S. Kumar and S. Bhattacharya. Implementation of floating point operations on fixed point processors — An optimization algorithm and comparative analysis. *IEEE 10th International conference on signal processing*. 2010, 409–412.

[25] J. A. Rice. *Mathematical Statistics and Data Analysis.* Third. Belmont, CA: Duxbury Press., 2006.

[26] A. Rico-Alvariño, J. Arnau and C. Mosquera. Balancing closed and open loop CSI in mobile satellite link adaptation. *2014 7th Advanced Satellite Multimedia Systems*

Conference and the 13th Signal Processing for Space Communications Workshop (ASMS/SPSC). 2014, 226–233. DOI: 10.1109/ASMS-SPSC.2014.6934548.

[27] I. A. Rumyancev and A. S. Korotkov. Survey on Beamforming Techniques and Integrated Circuits for 5G Systems. *2019 IEEE International Conference on Electrical Engineering and Photonics (EExPolytech)*. 2019, 76–80.

[28] O. Sarbishei and K. Radecka. On the Fixed-Point Accuracy Analysis and Optimization of Polynomial Specifications. *IEEE Transactions on Computer-Aided Design of Integrated Circuits and Systems* 32.6 (2013), 831–844.

[29] S. Schwarz, R. Heath and M. Rupp. Single-user MIMO versus multi-user MIMO in distributed antenna systems with limited feedback. *EURASIP Journal on Advances in Signal Processing* 2013 (Dec. 2013). DOI: 10.1186/1687-6180-2013-54.

[30] M. Shafi, A. F. Molisch, P. J. Smith, T. Haustein, P. Zhu, P. De Silva, F. Tufvesson, A. Benjebbour and G. Wunder. 5G: A Tutorial Overview of Standards, Trials, Challenges, Deployment, and Practice. *IEEE Journal on Selected Areas in Communications* 35.6 (2017), 1201–1221. DOI: 10.1109/JSAC.2017.2692307.

[31] Da-Shan Shiu, G. J. Faschini, M. J. Gans and J. M. Kahn. Fading correlation and its effect on the capacity of multi-element antenna systems. *ICUPC '98. IEEE 1998 International Conference on Universal Personal Communications. Conference Proc. (Cat. No.98TH8384)*. Vol. 1. 1998, 429–433 vol.1.

[32] M. Sharif and B. Hassibi. A Comparison of Time-Sharing, DPC, and Beamforming for MIMO Broadcast Channels With Many Users. *IEEE Transactions on Communications* 55.1 (2007), 11–15.

[33] Shengli Zhou and G. B. Giannakis. Optimal transmitter eigen-beamforming and space-time block coding based on channel correlations. *IEEE Transactions on Information Theory* 49.7 (2003), 1673–1690.

[34] N. Shimakawa and Y. Iwanami. A diversity order design of linearly precoded MU-MIMO downlink system. *2016 IEEE Region 10 Conference (TENCON)*. 2016, 1937–1940.

[35] Q. H. Spencer, A. L. Swindlehurst and M. Haardt. Zero-forcing methods for downlink spatial multiplexing in multiuser MIMO channels. *IEEE Transactions on Signal Processing* 52.2 (2004), 461–471.

[36] Taesang Yoo and A. Goldsmith. On the optimality of multiantenna broadcast scheduling using zero-forcing beamforming. *IEEE Journal on Selected Areas in Communications* 24.3 (2006), 528–541.

[37] E. Telatar. Capacity of Multi-antenna Gaussian Channels. *European Transactions on Telecommunications* 10.6 (1999), 585–595. DOI: 10.1002/ett.4460100604.

[38] D. Tse and P. Viswanath. *Fundamentals of Wireless Communication*. USA: Cambridge University Press, 2005. ISBN: 0521845270.

[39] B. D. Van Veen and K. M. Buckley. Beamforming: a versatile approach to spatial filtering. *IEEE ASSP Magazine* 5.2 (1988), 4–24.

[40] M. Vu and A. Paulraj. MIMO wireless linear precoding. *IEEE Signal Processing Magazine*. 2007, 86–105. DOI: 10.1109/MSP.2007.904811.

[41] N. Wang, P. Agathoklis and A. Antoniou. A Subspace Multiuser Beamforming Algorithm for the Downlink in Mobile Communications. *IEEE Transactions on Circuits and Systems II: Express Briefs* 53.8 (2006), 753–757.

[42] A. Wiesel, Y. C. Eldar and S. Shamai. Zero-Forcing Precoding and Generalized Inverses. *IEEE Transactions on Signal Processing* 56.9 (2008), 4409–4418.

[43] Ying-Chang Liang and F. P. S. Chin. Downlink channel covariance matrix (DCCM) estimation and its applications in wireless DS-CDMA systems. *IEEE Journal on Selected Areas in Communications* 19.2 (2001), 222–232.

[44] L. Zhang, Y. Zhang and W. Zhou. Floating-point to Fixed-point Transformation Using Extreme Value Theory. *2009 Eighth IEEE/ACIS International Conference on Computer and Information Science*. 2009, 271–276.